

# Nonstationary Spatial Process Models with Spatially Varying Covariance Kernels

Sébastien Coube-Sisqueille<sup>a,1</sup> \*, Sudipto Banerjee<sup>b,2</sup>, and Benoît Liquet<sup>a,c,3</sup>

<sup>a</sup> Laboratoire de Mathématiques et de leurs Applications,  
Université de Pau et des Pays de l'Adour, E2S-UPPA, Pau, France

<sup>b</sup> Department of Biostatistics, University of California, Los Angeles, United States of America

<sup>c</sup> School of Mathematical and Physical Sciences, Macquarie University, Sydney, Australia

<sup>1</sup> sebastien.coube@univ.pau.fr <sup>2</sup> sudipto@ucla.edu <sup>3</sup> benoit.liquet-weiland@mq.edu.au

## Abstract

Spatial process models for capturing nonstationary behavior in scientific data present several challenges with regard to statistical inference and uncertainty quantification. While nonstationary spatially-varying kernels are attractive for their flexibility and richness (see, e.g., Paciorek, 2003), their practical implementation has been reported to be overwhelmingly cumbersome because of the high-dimensional parameter spaces resulting from the spatially varying process parameters. Matters are considerably exacerbated with the massive numbers of spatial locations over which measurements are available. With limited theoretical tractability offered by nonstationary spatial processes, overcoming such computational bottlenecks require a synergy between model construction and algorithm development. We build a class of scalable nonstationary spatial process models using spatially varying covariance kernels. We present some novel consequences of such representations that befit computationally efficient implementation. More specifically, we operate within a coherent Bayesian modeling framework to achieve full uncertainty quantification using a Hybrid Monte-Carlo with nested interweaving. We carry out experiments on synthetic data sets to explore model selection and parameter identifiability and assess inferential improvements accrued from the nonstationary modeling. We illustrate strengths and pitfalls with a data set on remote sensed normalized difference vegetation index with further analysis of a lead contamination data set in the Supplement.

*Keywords:* Bayesian hierarchical models; Hybrid Monte-Carlo; Interweaving; Nearest-Neighbor Gaussian processes; Nonstationary spatial modeling.

---

\*The authors gratefully acknowledge *E2S: Energy and Environment Solutions*

# 1 Introduction

Bayesian hierarchical models for analysing spatially and temporally oriented data are widely employed in scientific and technological applications in the physical, environmental and health sciences (Cressie and Wikle, 2015; Banerjee et al., 2014; Gelfand et al., 2019). Such models are constructed by embedding a spatial process within a hierarchical structure,

$$[\text{data} \mid \text{process, parameters}] \times [\text{process} \mid \text{parameters}] \times [\text{parameters}], \quad (1)$$

which specifies the joint probability law of the data, an underlying spatial process and the parameters. The process in (1) is a crucial inferential component that introduces spatial and/or temporal dependence, allows us to infer about the underlying data generating mechanism and carry out predictions over entire spatial-temporal domains. Point-referenced spatial data, which will be our focus here, refer to measurements over a set of locations with fixed coordinates. These measurements are assumed to arise as a partial realization of a spatial process over the finite set of locations. Stationary Gaussian processes are conspicuous in spatial models. Stationarity imposes simplifying assumptions on the dependence structure of the process, which are unlikely to hold in most scientific applications.

Nonstationary spatial models attempt to relax such assumptions and deliver wide-ranging benefits to inference. For example, when variability in the data is a complex function of space composed of multiple locally varying processes, the customary stationary covariance kernels may be inadequate. Here, richer and more informative covariance structures in nonstationary processes, while adding complexity, may be more desirable by improving smoothing, goodness of fit and predictive inference. Nonstationary spatial models have been addressed by a number of authors (Higdon, 1998; Fuentes, 2002; Paciorek, 2003; Banerjee et al., 2008; Cressie and Johannesson, 2008; Lemos et al., 2009; Guhaniyogi et al., 2013; Yang and Bradley, 2021; Risser and Calder, 2015; Risser, 2016;

Fuglstad et al., 2015a; Gelfand et al., 2010, Chapter 9). The richness sought in nonstationary models have been exemplified in a number of the above references. Paciorek (2003) and Kleiber and Nychka (2012) introduce nonstationarity by allowing the parameters of the Matérn class to vary with location, yielding local variances, local ranges and local geometric anisotropies. While some of these approaches are related to ideas in modeling covariance matrices using covariates (see, e.g., Pourahmadi, 1999) and have been extended and further developed in a number of different directions including regularized inference, they have not been devised for implementation on massive spatial data sets in the order of  $10^5+$ . While recent developments in nonstationary models have addressed data sets in the order of hundreds (Risser and Calder, 2015; Ingebrigtsen et al., 2015; Heinonen et al., 2016) or thousands (Guhaniyogi et al., 2013; Fuglstad et al., 2015a) of locations, these are modest with respect to the size of commonly encountered spatial data (see the examples in Datta et al., 2016; Heaton et al., 2019; Katzfuss and Guinness, 2021). Bakka et al. (2019) proposed a novel “barrier” nonstationary model that achieves computational effectiveness by using simultaneous autoregression represented through a stochastic partial differential equation. Nonstationary models also suffer from unidentifiable parameters arising from complex space-varying covariance kernels, which yield weakly identifiable models that are difficult to estimate and interpret. This also complicates model evaluation and selection as inference is very sensitive to the specifications of the model.

We devise a new class of nonstationary spatial models for massive data sets that build upon Bayesian hierarchical models based on directed acyclic graphs (DAGs) such as the Nearest Neighbor Gaussian Process (NNGP) (Datta et al., 2016) and, more generally, Vecchia processes (Katzfuss and Guinness, 2021), which exploit their attractive computational and inferential properties (Finley et al., 2019). We focus upon spatially-varying

Matérn covariance kernels (e.g., [Paciorek, 2003](#); [Kleiber and Nychka, 2012](#)) by endowing the space-varying parameters with a low-dimensional Gaussian process. This achieves sparser representations than [Paciorek \(2003\)](#) or [Risser and Calder \(2015\)](#) and is a natural extension of the usual logarithmic prior for positive parameters such as the marginal variance, the noise variance, and the range when it is not elliptic. We embed these well-defined stochastic processes within a coherent hierarchical modeling framework as in [Heinonen et al. \(2016\)](#), but tailor our method towards modeling large data sets and capturing local anisotropy.

A key challenge is learning about the nonstationary covariance processes. This cannot be addressed solely using theoretical results (asymptotic theory for nonstationary processes are hardly accessible) or solely relying upon sophisticated algorithms (achieving convergence in high-dimensional parameter spaces will be unfeasible). Therefore, our approach relies upon some novel consequences of sparser representations in conjunction with a Hamiltonian Monte Carlo (HMC) algorithm adapted from [Heinonen et al. \(2016\)](#) to overcome computational impediments and analyze spatial data at massive scales. More specifically, we hybridize the approach of [Heinonen et al. \(2016\)](#) with the interweaving strategies of [Yu and Meng \(2011\)](#); [Filippone et al. \(2013\)](#). Our proposed method is able to achieve fully probabilistic inference on a latent nonstationary process which captures residual spatial behavior after accounting for spatial predictors. Our framework encompasses several simpler models as special cases. While theoretical properties of model selection based upon nonstationary features are analytically inaccessible, we conduct an array of computer experiments on synthetic data to demonstrate that our devised sparsity-inducing process models do not over-fit data generated from a simpler model. Instead, they degenerate towards a state corresponding to a simpler model.

The balance of the article proceeds as follows. [Section 2](#) outlines the covariance and

data models, and the properties of a nonstationary NNGP density, which are incorporated into a Bayesian hierarchical model presented in Section 3. Section 4 details the MCMC implementation of the model based upon a Gibbs sampler using interweaving in Section 4.2 and upon a Hamiltonian Monte Carlo algorithm in Section 4.3. Section 5 focuses on applications: experiments on synthetic data to test the properties of the model. We use the model to analyse a data set of lead contamination Hengl (2009) in the United States. Section 6 summarizes and points to future research. An elaborate accompanying Supplement offers key derivations, further details on algorithms and numerical results from simulation experiments.

## 2 Spatially-Varying Covariance Kernel Models

Let  $\mathcal{S} = \{s_1, s_2, \dots, s_n\}$  be a set of  $n$  spatial locations indexed in a spatial domain  $\mathcal{D}$ , where  $\mathcal{D} \subset \mathbb{R}^d$  with  $d \in \{1, 2, 3\}$ . For any  $s \in \mathcal{D}$  we envision a spatial regression model

$$z(s) = x(s)^\top \beta + w(s) + \epsilon(s) , \quad (2)$$

where  $z(s)$  represents a measurement at  $s$ ,  $x(s)$  is a  $p \times 1$  vector of predictors,  $\beta$  is the corresponding  $p \times 1$  vector of slopes,  $w(s)$  is a latent spatial process and  $\epsilon(s)$  is white noise attributed to random disturbances. In full generality, the noise will be modeled as heteroskedastic so that  $\epsilon(s) \stackrel{ind}{\sim} \mathcal{N}(0, \tau^2(s))$  while  $w(s)$  is customarily modelled using a Gaussian process over  $\mathcal{D}$ . Therefore,

$$w(\mathcal{S}) := (w(s_1), w(s_2), \dots, w(s_n))^\top \sim \mathcal{N}(0, \Sigma(\mathcal{S})) , \quad (3)$$

where the elements of the  $n \times n$  covariance matrix  $\Sigma(\mathcal{S})$  are determined from a spatial covariance function  $K(s, s')$  defined for any pair of locations  $s$  and  $s'$  in  $\mathcal{D}$ . In full generality the covariance function can accommodate spatially varying parameters to obtain

nonstationarity, which is our current focus. Therefore, the  $(i, j)$ -th element of  $\Sigma(\mathcal{S})$  is

$$\Sigma(s_i, s_j) = K(s_i, s_j) = \sigma(s_i)\sigma(s_j)K_0(s_i, s_j; \alpha(s_i), \alpha(s_j)), \quad (4)$$

where  $\sigma(s_1 \dots s_n) := \{\sigma(s_i) : i = 1, \dots, n\}$  is a collection of (positive) spatially varying marginal standard deviations,  $K_0(s, s'; \{\alpha(s), \alpha(s')\})$  is a valid spatial correlation function defined for any pair of locations  $s$  and  $s'$  in  $\mathcal{D}$  with two spatial range parameters  $\alpha(s)$  and  $\alpha(s')$  that vary with the locations. For two sets of locations  $a \in \mathcal{S}$  and  $b \in \mathcal{S}$ ,  $\Sigma(a, b)$  denotes the submatrix comprising the rows and columns of  $\Sigma$  whose indices correspond to  $a$  and  $b$  in  $\mathcal{S}$ , respectively. We also abbreviate  $\Sigma(a, a)$  into  $\Sigma(a)$ . These parameters can be either positive-definite matrices offering a locally anisotropic nonstationary covariance structure or positive real numbers specifying a locally isotropic nonstationary range. For example, [Paciorek \(2003\)](#) proposed a valid class of nonstationary covariance functions

$$K_0(s, s'; A(s), A(s')) = \frac{2^{d/2}|A(s)|^{1/4}|A(s')|^{1/4}}{|A(s) + A(s')|^{1/2}} K_i(d_M(s, s', (A(s) + A(s'))/2)), \quad (5)$$

where  $A(s)$  and  $A(s')$  are anisotropic spatially-varying range matrices,  $d$  is the dimension of the space-time domain,  $d_M(\cdot, \cdot, \cdot)$  is the Mahalanobis distance and  $K_i$  is an isotropic correlation function. If  $A(\cdot)$  does not vary by location, the covariance structure is anisotropic but stationary. A nonstationary correlation function is obtained by setting  $A(s) = \alpha(s)I_d$ ,

$$K_0(s, s'; \alpha(s), \alpha(s')) = \left( \frac{\sqrt{2}\alpha(s)^{1/4}\alpha(s')^{1/4}}{(\alpha(s) + \alpha(s'))^{1/2}} \right)^d K_i(d_E(s, s') / ((\alpha(s) + \alpha(s'))/2)), \quad (6)$$

where  $d_E(\cdot, \cdot)$  is the Euclidean distance (Mahalanobis distance with matrix  $I_d$ ).

Spatial process parameters in isotropic covariance functions are not consistently estimable under fixed-domain asymptotic paradigms ([Zhang, 2004](#)). Therefore, irrespective of sample size, no function of the data can converge in probability to the value of the parameter from an oracle model. Irrespective of how many locations we sample, the effect of the prior on these parameters will not be eliminated in Bayesian inference. This

can be addressed using penalized complexity priors to reduce the ridge of the equivalent range-marginal variance combinations to one of its points (Fuglstad et al., 2015b). The covariance function sharply drops to 0 so the observations that inform about the covariance parameters at a location tend to cluster around the site. Nonstationary models are significantly more complex. The parameters specifying the spatial covariance are functions over  $\mathcal{D}$ . These form uncountable collections and, hence, inference requires modeling them as spatial processes. This considerably exacerbates the challenges surrounding identifiability and inference for these completely unobserved processes. Asymptotic inference is precluded due to the lack of regularity conditions. Bayesian inference, while offering fully model-based solutions for completely unobserved processes, will also need to obviate the computational hurdles arising from weakly identified processes, which result in poorly behaved MCMC algorithms, and inference extensible to massive data sets.

The customary NNGP (Datta et al., 2016) specifies a valid Gaussian process in two steps. We begin with a “parent” process  $GP(0, K(s, s'))$  so that  $w(\mathcal{S})$  has the probability law in (3). Let  $f(w(\mathcal{S}) | \theta)$  be the corresponding joint density, where  $\theta$  denotes parameters in  $K(\cdot, \cdot)$ . First, we build a sparse approximation of this joint density. Using a fixed topological ordering of the points in  $\mathcal{S}$  we construct a nested sequence  $\mathcal{S}_{i-1} \subset \mathcal{S}_i$ , where  $\mathcal{S}_i = \{s_1, s_2, \dots, s_{i-1}\}$  for  $i = 2, 3, \dots, n$ . The joint density of the NNGP is given by  $\tilde{f}(w(\mathcal{S}) | \theta) = f(w(s_1) | \theta) \prod_{i=2}^n \tilde{f}(w(s_i) | w(\mathcal{S}_{i-1}), \theta)$  (also referred to as Vecchia’s approximation Vecchia, 1988; Stein et al., 2004), where

$$\tilde{f}(w(s_i) | w(\mathcal{S}_{i-1}), \theta) = f(w(s_i) | w(pa(s_i)), \theta), \quad (7)$$

and  $pa(s_i)$  comprises the parents of  $s_i$  from a DAG over  $\mathcal{S}$ . The parents in the DAG are often chosen as the nearest neighbours of  $s_i$  among  $s_1, \dots, s_{i-1}$ . This approximation defines a Gaussian Process whose covariance matrix can be expressed as  $(\tilde{R}^T \tilde{R})^{-1}$ . Each row of  $\tilde{R}$

is computed straightforwardly from the conditional distribution  $f(w(s_i) | w(pa(s_i)), \theta)$ . It follows that  $\tilde{R}$  is lower triangular and very sparse with its  $i$ -th row having nonzero entries only at the indices corresponding to  $pa(s_i)$  (Pourahmadi, 1999, 2007; Datta et al., 2016; Katzfuss and Guinness, 2021). Prediction at unobserved locations is achieved by appending them sequentially as new nodes with edges connecting the new locations to its nearest neighbors from the preceding nodes already in the DAG. This results in the predictive distribution  $\prod_{i=1}^{n_{pred}} f(w(\tilde{s}_i) | w(pa(\tilde{s}_i)), \theta)$ , where  $\tilde{s}_i$  are a topologically sorted sequence of locations where predictions are sought (see, e.g., Datta et al., 2016; Finley et al., 2019; Katzfuss et al., 2020, for scalable spatial interpolation and prediction).

We obtain  $\tilde{f}(w(\mathcal{S}) | \theta(\mathcal{S})) = f(w(s_1) | \theta(s_1)) \prod_{i=2}^n \tilde{f}(w(s_i) | w(\mathcal{S}_{i-1}), \theta(\mathcal{S}_i))$  by applying (7) to spatially varying parameters, where  $\theta(s)$  is a vector comprising the covariance function parameters at  $s$  and  $\theta(\mathcal{S}) = (\theta(s_1)^T, \theta(s_2)^T, \dots, \theta(s_n)^T)^T$  is a  $(\sum_{i=1}^n |\theta(s_i)|) \times 1$  vector. We build scalable nonstationary processes by exploiting the following key property (see Section S1.1 of the Supplement for the derivation),

$$\tilde{f}(w(s_i) | w(\mathcal{S}_{i-1}), \theta(\mathcal{S})) = f(w(s_i) | w(pa(s_i)), \theta(s_i \cup pa(s_i))) , \quad (8)$$

where the NNGP density is derived using covariance kernels in (5) and (6), both of which accommodate spatially-variable parameters  $\theta(\mathcal{S})$ . Equation (8) reveals a crucial property that the the NNGP will reduce the dimension of conditional sets from  $w(\mathcal{S}_{i-1})$  to  $w(pa(s_i))$  and from  $\theta(\mathcal{S})$  to  $\theta(s_i \cup pa(s_i))$ .

Another useful property relates the NNGP derived from the covariance function in (4) and its corresponding correlation function. Let  $\tilde{R}_0$  be the NNGP factor obtained from the precision matrix using the correlation function  $K_0(\cdot)$  instead of the covariance function  $K(\cdot)$  and let  $\sigma(\mathcal{S}) = (\sigma(s_1), \sigma(s_2), \dots, \sigma(s_n))^T$ . Then,  $\tilde{R} = \tilde{R}_0 \text{diag}(\sigma(\mathcal{S}))^{-1}$ , where  $\text{diag}(\sigma(\mathcal{S}))$  is the diagonal matrix with elements  $\sigma(s_i)$ ; see the Section S1.2 of the Supplement for the

derivation. The logarithm  $N(w(\mathcal{S}) | 0; \tilde{\Sigma}(\mathcal{S}; \theta))$  is computed up to a constant as

$$-\sum_{i=1}^n \log \left( (\tilde{R}_0)_{i,i} / \sigma(s_i) \right) - \frac{1}{2} w^T \text{diag}(\sigma(\mathcal{S}))^{-1} \tilde{R}_0^T \tilde{R}_0 \text{diag}(\sigma(\mathcal{S}))^{-1} w, \quad (9)$$

exploiting cheap expressions for the determinant of  $\tilde{R}$ . Furthermore, the topological ordering heuristics explored by Guinness (2018) hold for NNGP specifications in (5) and (6).

### 3 Hierarchical space-varying covariance models

We extend (2) to accommodate replicated measurements at each location. If  $z(s, j)$  is the  $j$ -th measurement at location  $s$ , where  $j = 1, 2, \dots, n_s$ , and  $z(s)$  is the  $n_s \times 1$  vector of all measurements at location  $s$ , then (2) is modified to  $z(s) = X(s)^T \beta + 1_{n_s} w(s) + \epsilon(s)$ , where  $X(s)^T$  is  $n_s \times p$  with the values of predictors or design variables corresponding to each location  $s$ ;  $1_{n_s}$  is the  $n_s \times 1$  vector of ones;  $\epsilon(s)$  is an  $n_s \times 1$  vector with  $j$ -th element  $\epsilon(s) \sim N(0, \text{diag}(\tau^2(s)))$ , where  $\tau^2(s) = (\tau_1^2(s), \dots, \tau_{n_s}^2(s))^T$  is  $n_s \times 1$ ; and  $\beta$  and  $w(s)$  are exactly as in (2). Note that  $X(s)^T$  can include predictors that do not vary within  $s$ , e.g., elevation, and that can vary within the spatial location, e.g., multiple technicians can record measurements at  $s$  and the technician's indicator may be used as a covariate.

We build a hierarchical space-varying covariance model over a set of spatial locations  $\mathcal{S} = \{s_1, \dots, s_n\}$  so the total number of measurements available for  $z(s)$  is  $|z| = \sum_{i=1}^n n_{s_i}$ . We propose the following hierarchical framework,

$$\underbrace{[z | \beta, w(\mathcal{S}), \tau^2(\mathcal{S})]}_{(a)} \times \underbrace{[w(\mathcal{S}) | \theta(\mathcal{S})]}_{(b)} \times \underbrace{[\theta(\mathcal{S}) | \beta_\theta, \gamma_\theta]}_{(c) \text{ and } (d)} \times \underbrace{[\tau^2(\mathcal{S}) | \gamma_\tau]}_{(e) \text{ and } (f)} \times \underbrace{[\gamma_\theta, \gamma_\tau, \beta_\theta, \beta_\tau]}_{(g)}, \quad (10)$$

where  $[\cdot]$  denotes probability distributions. These symbolic blocks are modeled as below:

$$\begin{aligned}
(a) \quad & z \sim N(X\beta + Mw(\mathcal{S}), \text{diag}(\tau^2(\mathcal{S}))) ; & (b) \quad & w(\mathcal{S}) \sim N(0, \tilde{\Sigma}(\mathcal{S}; \theta(\mathcal{S}))) ; \\
(c) \quad & \log(\theta(\mathcal{S})) = X_\theta(\mathcal{S})\beta_\theta + W_\theta(\mathcal{S}) ; & (d) \quad & W_\theta(\mathcal{S}) \sim N(0, \zeta_{\gamma_\theta}) ; \\
(e) \quad & \log(\tau^2(\mathcal{S})) = X_\tau(\mathcal{S})\beta_\tau + MW_\tau(\mathcal{S}) ; & (f) \quad & W_\tau(\mathcal{S}) \sim N(0, \zeta_{\gamma_\tau}) ; \\
(g) \quad & \{\gamma_\theta, \gamma_\tau, \beta_\theta, \beta_\tau, \beta\} \sim p(\cdot, \cdot, \cdot, \cdot, \cdot) ,
\end{aligned} \tag{11}$$

where in (11(a))  $z$  denotes the  $|z| \times 1$  vector of all measurements,  $X$  is  $|z| \times p$  obtained by stacking up  $X(s_i)^\top$  over the  $n$  locations in  $\mathcal{S}$ ,  $\beta$  is the corresponding vector of regression coefficients, and  $\text{diag}(\tau^2(\mathcal{S}))$  is a diagonal matrix with elements of the  $|z| \times 1$  vector  $\tau^2(\mathcal{S}) = (\tau^2(s_1)^\top, \tau^2(s_2)^\top, \dots, \tau^2(s_n)^\top)^\top$  along the diagonal. The matrix  $M$  is a  $|z| \times n$  matching matrix with elements  $M_{i,j} = 1$  if the  $i$ -th element of  $z$  corresponds to the  $j$ -th spatial location and 0 otherwise. We preclude an observation from being obtained in two spatial locations at the same time. Hence, each row of  $M$  has *exactly* one term equal to one. Also, since there is at least one observation in each location, each column of  $M$  has *at least* one term equal to one. This yields (2) with  $|z| = n$  and  $M$  as a permutation matrix.

In (11(b)), the distribution of  $w(\mathcal{S})$  is specified using (9) as described in Section 2. Equations (11(c)) and (11(e)) specify models for the space-varying parameters  $\theta(\mathcal{S})$  and  $\tau^2(\mathcal{S})$ , respectively, with (11(d)) and (11(f)) providing the distributional specifications. The dimension of  $\tau^2(\mathcal{S})$  for fully heteroskedastic specifications is  $|z| \times 1$  while  $\theta(\mathcal{S}) = (\theta(s_1)^\top, \dots, \theta(s_n)^\top)^\top$  is a vector whose dimension will depend upon the dimension of each  $\theta(s_i)$  in the model specification. The quantities  $\zeta_{\gamma_\theta}$  and  $\zeta_{\gamma_\beta}$  denote covariance matrices depending on parameters  $\gamma_\theta$  and  $\gamma_\beta$  according to the particular model we pursue. Furthermore, each  $\theta(s_i)$  is a  $d \times d$  matrix in anisotropic range models, whence (11(c)) is a matrix-variate linear model. We will revisit this adaptation in greater detail below. Both  $X$  and  $X_\tau$  have  $|z|$  rows that vary with measurements, while  $X_\theta(\mathcal{S})$  has  $n$  rows correspond-

ing to the spatial sites. Specifying  $X_\theta$  is necessary to ensure that  $w(s)$  is well-identified, while  $X_\tau$  accommodates modeling errors within a spatial site, e.g. to account for variation among measurements from different technicians within a single spatial location. Finally, (11(g)) completes the hierarchical specification with distributions on the hitherto unspecified parameters introduced earlier in (11).

The models in (11(c) and (e)) require some further discussion. Let  $|\theta(s)|$  be the dimension of the space-varying covariance kernel parameters at location  $s$ . Therefore,  $|\theta(\mathcal{S})|$  is  $O(n)$  and so is  $|W_\theta(\mathcal{S})|$ , which results in an apparently insurmountable estimation problem when  $n \gg 10^4+$ . One approach is to assign an NNGP prior for  $W_\theta(\mathcal{S})$ , as was done for  $w(\mathcal{S})$  in Section 2. This, as has been discussed in Section 2, approximates the parent Gaussian process while offering massive computational benefits and can deliver estimates of the random field for  $\theta$  that are almost indistinguishable from the parent. Another option is a low rank process for each element in  $W_\theta(s)$ . Writing  $W_\theta(s) = (W_{\theta,1}(s), W_{\theta,2}(s), \dots, W_{\theta,|\theta(s)|}(s))^T$  as a  $|\theta(s)| \times 1$  vector, we model its  $j$ -th element  $W_{\theta,j}(s) = \sum_{k=1}^p B_{\theta,j,k}(s)u_k$  for  $j = 1, 2, \dots, |\theta(s)|$ , where  $B_{\theta,j,k}(s)$  is a basis functions and  $u = (u_1, u_2, \dots, u_p)^T$  is a  $p \times 1$  vector of basis coefficients. Therefore,  $W_\theta(s) = B_\theta(s)u$ , where  $B_\theta(s)$  is  $|\theta(s)| \times p$  with elements  $(B_{\theta,j,k}(s))$  and  $u \sim N(0, \gamma_\theta I_p)$  is  $p \times 1$ . In particular, the basis functions can be constructed as in Banerjee et al. (2008) using the conditional expectation of a full-rank Gaussian Process  $\mathbb{E}[W_\theta(s) | W_\theta(\mathcal{S}^*)]$ , where  $\mathcal{S}^*$  is a smaller set of  $p$  ‘‘knots’’ in the domain (see Section S6 of the Supplement). We provide a few remarks on the selection of knots. The knots can be found as the centers of a K-means clustering, thereby allowing the user to specify only the desired number of knots. Our package vignette offers a quick look at how the PP samples behave using our spatial plotting functions. We point out that Guhaniyogi et al. (2011) have undertaken a rather thorough

investigation of adaptive knot selection in predictive process models. For now, our recommendation is to keep the PP as simple as possible in the interest of being able to work with a very large number of high-level parameters. Collecting over locations in  $\mathcal{S}$ , we obtain  $W_\theta(\mathcal{S}) = B_\theta(\mathcal{S})u$  where  $B_\theta(\mathcal{S})$  is  $|\theta(\mathcal{S})| \times p$  with  $B_\theta(s_i)$  as the  $i$ -th block,  $i = 1, 2, \dots, n$ . Therefore,  $W_\theta(\mathcal{S}) \sim \mathcal{N}(0, \gamma_\theta B(\mathcal{S})B^\top(\mathcal{S}))$ . While the variance parameter is modeled as  $\log \gamma_\theta \sim U(\cdot, \cdot)$ , where  $U(\cdot, \cdot)$  represents a uniform prior, we leave the spatial range of  $W_\theta$  to be specified and fixed by the modeler due to limited information about the spatial range and marginal variance of a Gaussian process (Zhang, 2004).

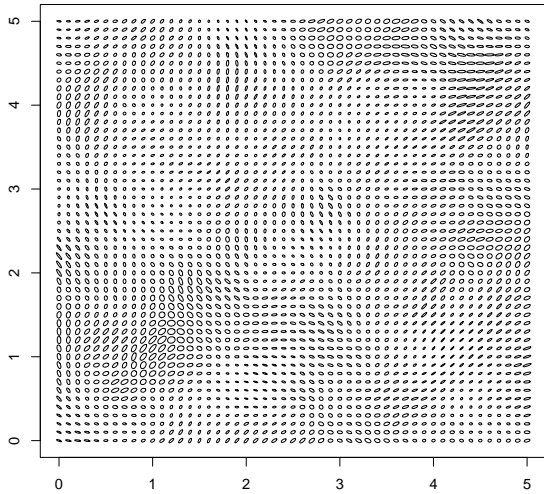
This framework enables learning about  $\theta(s)$  and  $\tau(s)$  by borrowing information from measurements of explanatory variables,  $X_\theta(s)$  and  $X_\tau(s)$  that drive nonstationary behavior with fixed effects  $X_\theta\beta_\theta$  and  $X_\tau\beta_\tau$ , respectively. If such variables are absent, then  $X_\theta$  and  $X_\tau$  consist of an intercept only. The associated regression coefficients are customarily assigned a Gaussian prior specified by the user. The structure of the fixed effects and the random effects is, therefore, very similar with  $B$  playing the same role as  $X_\theta$ , the difference between them being that the prior variance of  $\tilde{W}_\theta$  is estimated by the model while the prior variance of  $\beta_\theta$  is fixed by the user. If  $\theta(s)$  is a matrix, as occurs with anisotropic range parameters in (6), the above framework is easily modified. Let  $\theta(s) = A(s)$  be a  $d \times d$  positive definite matrix with positive eigenvalues  $\lambda_1(s), \lambda_2(s), \dots, \lambda_d(s)$ . If  $A(s) = P(s)\Lambda(s)P(s)^\top$  is the spectral decomposition, then we use the matrix logarithm  $\log A(s) = P(s)\log(\Lambda(s))P(s)^\top$ , where  $\log(\Lambda(s))$  is the diagonal matrix with  $\log(\lambda_i(s))$  for  $i = 1, 2, \dots, d$  as the diagonal elements. The matrix logarithm maps the positive definite matrices to the symmetric matrices (but not necessarily positive definite) and  $(\log(A(s)))^{-1} = -\log(A(s))$ , which is convenient for parametric specifications. Let  $\text{symmat}(\cdot)$  denote the symmetric matrix operator (or the inverse map of the half-vectorization operator  $\text{vech}(\cdot)$ ) that fills the upper

and lower triangles of a matrix from a vector of suitable length to form a symmetric matrix.

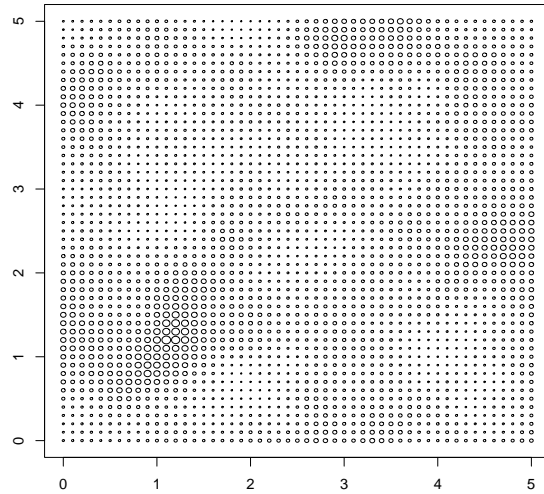
The model for  $\log(\theta(s))$  in (11) now is

$$\log(A(s)) = \text{symmat}((X_A(s)\beta_A + W_A(s))M(d)) , \quad (12)$$

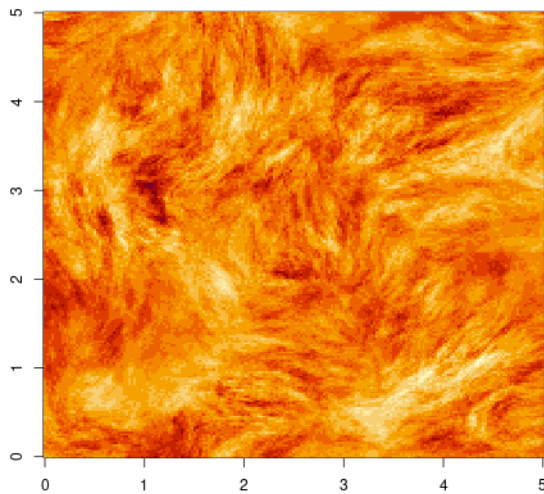
where  $X_A(s)\beta_A + W_A(s)$  is a vector of length  $d \times (d + 1)/2$ ,  $s \in \mathbb{R}^d$ ,  $M$  is a square matrix of size  $d(d + 1)/2$ , and  $\beta_A$  is  $n_{X_A} \times d(d + 1)/2$ . The symmetry of  $\log(A(s))$  leads to the positive-definiteness of  $A(s)$ . For the sake of interpretation, we apply a change of basis to the half-vectorization of  $\log(A(s))$  using  $M(d)$ . The first row of  $M(d)$  is  $\text{vech}(I_{d \times (d+1)/2} / \sqrt{d \times (d+1)/2})$  and the other rows are obtained by applying  $\text{vech}(\cdot)$  to any completion of basis of the symmetric matrices from  $I_{d \times (d+1)/2} / \sqrt{d \times (d+1)/2}$ . The first coefficient of  $X_A(s)\beta_A + W_A(s)$  controls the determinant of  $A(s)$ , which yields the product of the range ellipse axis lengths, and will inflate and deflate the range of the ellipse without changing its shape. The other components will rotate and squash the ellipse without changing the product of the lengths of its axes. Further, we specify  $W_A(s) = B_A(s)\tilde{W}_A$ , where  $\tilde{W}_A$  is  $p \times d(d + 1)/2$ . The variance parameter  $\gamma_A$  is  $d(d + 1)/2 \times d(d + 1)/2$  with  $\text{vec}(\tilde{W}_A) \sim \mathcal{N}(0, \gamma_A \otimes I_p)$ . We can now persist with the hyperpriors presented earlier. A Gaussian prior is assigned to  $\beta_A$ , and a Uniform prior to the eigenvalues of  $\gamma_A$ . If only the first columns of  $\beta_A$  and  $\tilde{W}_A$  are non-null, then this model is effectively equal to the locally-isotropic nonstationary range model presented earlier. If  $\tilde{W}_A$  is null and only the first row of  $\beta_A$  is non-null, then the model is anisotropic, but stationary. If only the upper-left coefficient in  $\tilde{W}_A$  is non-null, then the model is stationary and isotropic. An illustration of the kind of distributions obtained thus is presented in Figure 1. Figure 1(a) presents range ellipses generated with (12), while Figure 1(b) presents range ellipses generated with 11(d). Figures 1(c) and 1(d) represent one of their respective Gaussian process sample paths obtained with (11)(b).



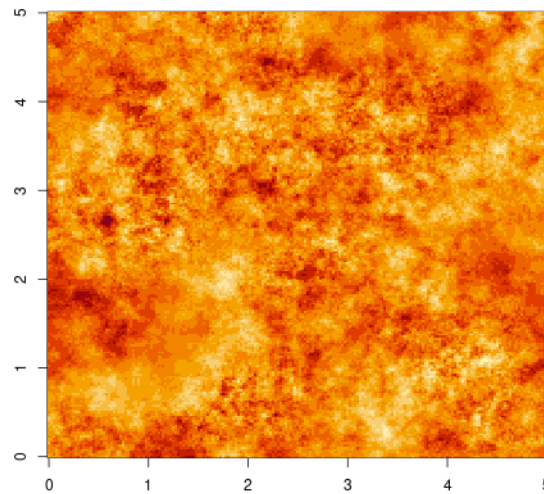
(a) Ellipses obtained with matrix log GP



(b) Circles obtained with scalar log GP



(c) GP samples corresponding to the ellipses



(d) GP samples corresponding to the circles

Figure 1: Range ellipses and GP samples induced by the log-GP and matrix log-GP priors

We conclude this section with a few remarks. There is little to argue about the complexity encoded in (10) and (11). Inference problems in even simpler stationary models is encumbered by well-known issues of model identifiability (Stein, 1999; Zhang, 2004; Tang et al., 2021). These issues are exacerbated in nonstationary models with almost no theoretical tractability. It is, therefore, crucial to model the latent processes with reasonable priors. For example, while a non-informative prior on  $\beta$  is reasonable, more informative priors for  $\beta_\theta$  and  $\beta_\tau$  would be desirable on the basis of information in  $X_\theta$  and  $X_\tau$ . However, in the absence of such information, even with only intercepts in these matrices, we are able to demonstrate fairly robust inference (see Sections 5.1 and 5.2) with regard to the nonstationary processes. The fixed effects and the spatially-driven effects for the range and the field’s marginal variance cannot be independent. Indeed, some spatial incoherence of these effects is very likely to cause identifiability issues between the parameter field and the latent field. We refer the reader to the supplement and vignette for details.

## 4 Markov chain Monte Carlo algorithms

### 4.1 Outline

We devise a Gibbs sampler, where each parameter is updated conditionally on the rest, which is further improved by introducing appropriate updating methods built from other works or developed in this article. The latent field  $w(\mathcal{S})$  is sampled using the blocked update (Datta et al., 2016, Section 4.1) in order to mitigate spatial auto-correlation. The regression coefficients  $\beta$  are updated using the “Interweaving” method proposed in Coube-Sisquille and Liquez (2021). The low-rank formulation of  $W_\theta$  and  $W_\tau$  ensures that only the basis coefficients need to be updated. These are block-sampled with their respective counterparts

$\beta_\theta$  and  $\beta_\tau$ . The basis coefficients for  $W_\theta$  are updated using an interweaving strategy with respect to the latent field  $w(\cdot)$  inspired from (Filippone et al., 2013); see Section 4.2. We sample the basis coefficients for  $W_\tau$  from their full conditional distributions. In both cases, Hybrid Monte Carlo or HMC (see Section 4.3) is used yielding, respectively, a “HMC-within-interweaving” for  $W_\theta$  and “HMC-within-Gibbs” for  $W_\tau$ . The higher-level parameters  $\{\gamma_\theta, \gamma_\tau\}$ , are successively updated using an interweaving strategy on their respective latent fields. In the case of  $\gamma_\theta$ , this interacts with the interweaving on  $w$ . The resulting algorithm is outlined in Section S3.3 of the Supplement.

## 4.2 Ancillary-Sufficient Interweaving Strategy

The problem of high correlation between latent fields and higher-level parameters is familiar in stationary spatial models, and several solutions exist such as blocking (Knorr-Held and Rue, 2002), collapsing (Finley et al., 2019) or Interweaving (Filippone et al., 2013). Interweaving exploits the discordance between two parametrizations of a latent field to sample high-level parameters. When these two parametrizations are an ancillary-sufficient couple, we have an Ancillary-Sufficient Interweaving Strategy (AS-IS); see Yu and Meng (2011) and also Section S3.1 in the Supplement.

In our application, we interweave the whitened and natural parametrizations of the latent field  $w(\mathcal{S})$  from (11)(a) in order to update the higher-level parameters  $W_\theta(\mathcal{S})$  and  $\beta_\theta$  impacting the covariance structure decomposed in (11)(c) and (12). The so-called *natural parametrization* of the latent field is found in the decomposition (11)(a) and is a sufficient parametrization. The *whitened parametrization* of the latent field is ancillary and is obtained by multiplying the natural parametrization with the right NNGP factor of its prior precision matrix from (11)(b):  $w^*(\mathcal{S}) = \tilde{R}w(\mathcal{S})$  so that the prior distribution (11)(b) be-

comes a standard normal distribution. The covariance parameters have no effect anymore on the prior distribution of the latent field. In turn, they acquire a role in the decomposition of the data. In (11)(a),  $w(s_i)$  is replaced by the  $i$ -th element of  $\tilde{R}^{-1}w^*(\mathcal{S})$ , while 11(b) is replaced by  $w^*(\mathcal{S}) \sim \mathcal{N}(0, I_{|\mathcal{S}|})$ . Further developments concerning the behavior of  $w^*$  are available in Coube-Sisqueille (2021).

The parameter of interest is sampled in two steps, one for each parametrization of the latent field. These individual steps can be full conditional draws, random walk Metropolis steps or, as in our case, Hybrid Monte-Carlo (HMC) steps. Hence, two potentials will be derived for the HMC steps of each parameter. Note that  $\gamma_\theta$  and  $\gamma_\tau$  are themselves covariance parameters for the latent fields  $W_\theta$  (11(d)) and  $W_\tau$  (11(f)). In order to update  $\gamma_\theta$  and  $\gamma_\tau$ , interweaving is used by treating  $W_\theta$  and  $W_\tau$  as latent fields and using their respective whitened parametrizations. In the case of  $\gamma_\theta$ , *nested interweaving* allows us to use the whitened parametrizations of  $\tilde{W}_\theta(\mathcal{S})$  and  $w(\mathcal{S})$ .

### 4.3 Hybrid Monte-Carlo

Hybrid Monte-Carlo (HMC) (Neal et al., 2011) has been implemented successfully by Heinonen et al. (2016) for nonstationary Gaussian processes. Our approach differs in two aspects. First, we use NNGP instead of full GP and, hence, differentiate the NNGP-induced potential, which is non-trivial. Second, we use an ‘‘HMC within AS-IS’’ algorithm and must find the gradients of the potential for the covariance parameters using both ancillary and sufficient parametrizations. We jointly update the Predictive Process coefficients and the regression coefficients  $\beta_\tau$  and  $\tilde{W}_\tau$  in (11)(e),  $\beta_\theta$  and  $\tilde{W}_\theta$  in (11)(c), or  $\beta_A$  and  $\tilde{W}_A$  in (12). This method is especially useful for the range parameters since it avoids an unfeasible Metropolis-within-Gibbs sweep over  $\beta_\alpha$ . The method applies to  $\alpha$ ,  $\sigma$  or  $\tau$ , so we

use “ $\lambda$ ” as a portmanteau. We differentiate  $H = -g(\beta_\lambda, W_\lambda) - \log(p(\beta_\lambda)) - \log(p(\tilde{W}_\lambda|\gamma_\lambda))$ . Here,  $g(\cdot, \cdot)$  depends on the role of  $\lambda$  in the model and the chosen parametrization of the latent field in interweaving;  $p(\cdot)$  denotes prior distributions whose parameters are either set by the user in the case of  $\beta_\lambda$  or estimated by the model in the case of  $\tilde{W}_\lambda$ . We express  $g(\beta_\lambda, W_\lambda) = h \circ \log(\lambda)(\beta_\lambda, W_\lambda)$ ,  $\log(\lambda)(\cdot, \cdot)$  being a function that links  $\beta_\lambda, \tilde{W}_\lambda$  and the logarithm of  $\lambda$  following (11)(c), (11)(e), or (12). Using the Jacobian chain rule on  $g(\beta_\lambda, \tilde{W}_\lambda)$ , the gradient can then be written as

$$\nabla_{\beta_\lambda, \tilde{W}_\lambda} H = -\nabla_{\beta_\lambda} \log(p(\beta_\lambda)) - \nabla_{\tilde{W}_\lambda} \log(p(\tilde{W}_\lambda|\gamma_\lambda)) - J_{\beta_\lambda, \tilde{W}_\lambda}^T \log(\lambda) \cdot \nabla_{\log(\lambda)} h(\log(\lambda)).$$

Recognizing that  $\log(\lambda)$  varies linearly with respect to  $\beta_\lambda$  and  $\tilde{W}_\lambda$ , we get  $J_{\beta_\lambda, \tilde{W}_\lambda}^T \log(\lambda) = (X_\lambda|B)^T$ . The details for computing the gradient of  $h_\lambda$  are supplied in Section S4.1 of the Supplement. The cost of gradient computation depends on the specific parameter. While the noise variance boils down to a product of independent densities, the range and marginal variance of the latent field involve  $\tilde{R}$  for multiplication and solving. These operations, which would be unfeasible with dense matrices, remain efficient because of the triangular and sparse  $\tilde{R}$  (Datta et al., 2016). Furthermore, (9) allows for efficient computation of the gradient for parameters related to the field’s variance. For the range, (8) is critical to establish the fact that one range parameter only affects its children in the DAG, allowing for sparse differentiation, in synergy with the computation of the coefficients of  $\tilde{R}$ . Overall, the cost of the gradient computation depends linearly on the number of observations.

## 5 Applications of the model

Our model and codes are available from the public repository <https://github.com/SebastienCoube/Nonstat-NNGP> and includes an extensive vignette for practitioners.

## 5.1 Synthetic experiments

In our synthetic experiments, we generate data sets ranging from stationary specifications to those exhibiting varying degrees of nonstationarity using (11). We randomly sample 12000 locations on a square with side length 5 using an Uniform distribution. Then, the regression coefficients in (11) (a), (c), and (e) are fixed. The only predictor in  $X$  is an intercept. We fix  $\beta = 0$  and  $\beta_\tau = 0$  in (11)(a) and (11)(e), respectively. In the stationary configuration, the noise and the latent field have same marginal variances equal to  $\exp(0) = 1$ . For  $\beta_\theta$  in (11)(c), the intercept coefficient for the range is set to  $\log(0.1) \approx -2.3$  while that for the smoothness is 1.5. In the anisotropic cases, the intercept is set to 0. These parameters are the same for all runs, including our non-stationary examples.

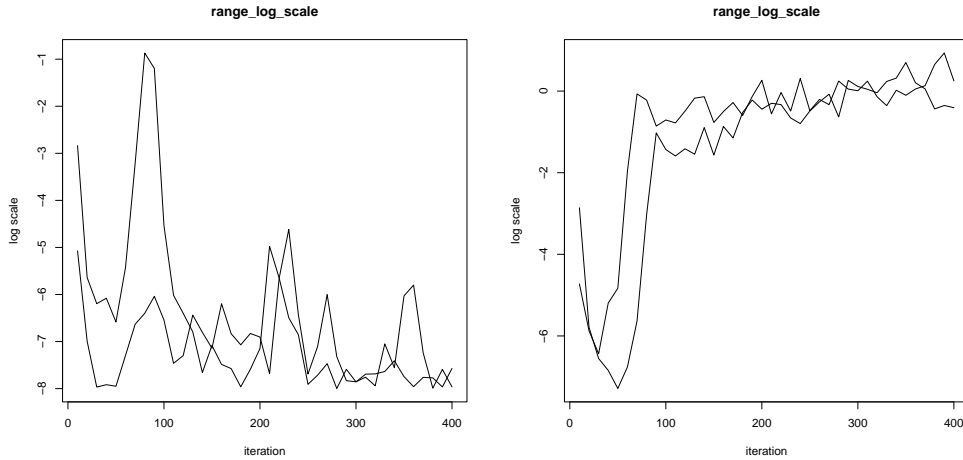
The log-scale parameters  $\gamma_\theta, \gamma_\tau$  from (11)(g) change. In a stationary model, they are set to 0. In a nonstationary model, they are set to 1. After this, all the parameters are generated randomly, following their respective prior distributions (d), (f), (b) and (a) in (11). We subsequently fit several candidate models to the synthetic data we generated. We consider four situations: (i) “under-modeling” when the model is less complex than the data generating process; (ii) “over-modeling” which is the opposite of (i); (iii) the so-called “correct” (or “right”) modeling, when the specifications of the model and the data are the same; and (iv) models that fall in none of the above three categories. Several indicators were monitored: the Deviance Information Criterion (DIC) (Spiegelhalter et al., 1998), the mean square error (MSE) of the predicted field at unobserved sites, the MSE of the smoothed field at observed sites, and the MSE of the smoothed covariance parameters. We did not include predictions of the covariance parameters due to the smoothing of the PP. Further details are supplied in Section S5 of the Supplement.

Since the stationary models emerge as special cases of nonstationary models, we can

informally detect over-modeling from the MCMC chains without requiring to wait for full convergence by looking at the samples of the log-GP variance  $\gamma$ . This is done using trace plots, presented in Figures 2 and 3, where each curve corresponds to one Markov chain. When the data set is stationary while the model is nonstationary,  $\gamma$  drops to very small values, such as in Figures 2(a) and 3(a), effectively inducing a stationary latent field. When the range is locally isotropic, but nonstationary, we observe the behavior of Figure 2(b), where the parameter controlling the range’s log-variance takes high values. In Figure 3, the first component, labeled “determinant”, controls the variance of the determinant of the range ellipses, allowing them to inflate or deflate over space, such as the parameters monitored in Figure 2. Two other parameters, labeled “anisotropy”, allow the range ellipses to squash (with area preservation) and change orientation. In Figure 3(b), only “determinant” is high. Hence, the ellipses may change their size, but not their shape, practically retrieving the locally isotropic covariance. However, here a simpler model is preferable.

The locally isotropic range and the heteroskedastic marginal variance of the process seem to be poorly identified. If we apply a misspecified model with one nonstationary parameter to a data set generated with the other parameter as nonstationary, then we still obtain inference competitive with the true model. The same finding holds for data sets where both parameters are nonstationary and we specify only one as nonstationary. However, if none are specified as nonstationary when at least one ought to be, the performance deteriorates. See Section S5.4 of the Supplement for details.

It is clear that the loss of performance caused by using a stationary model (the bottom rows in the tables of Section S5 in the Supplement) is usually lesser than the loss caused by a poorer model formulation (in red in the tables) or other under-modeling cases (in gray). From these results, we proffer that a nonstationary formulation should always accommodate



(a) Data with stationary range

(b) Data with nonstationary range

$(\gamma_\alpha = 0)$

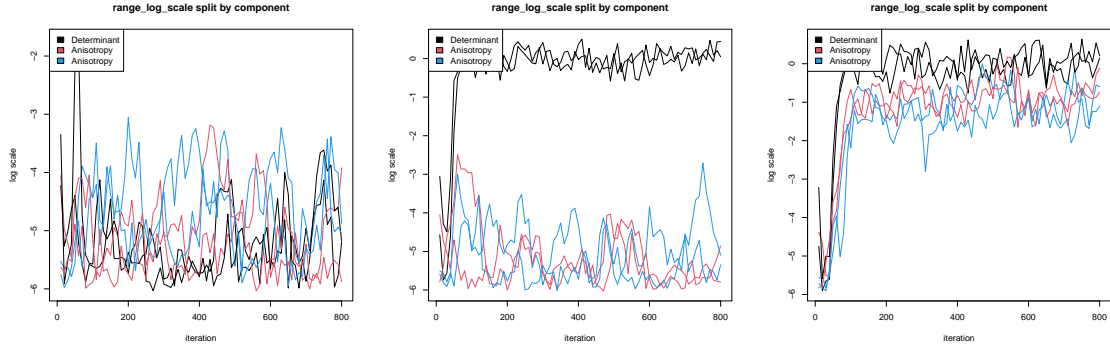
$(\gamma_\alpha = 1)$

Figure 2: MCMC samples of the range PP log-variance parameter  $\log(\gamma_\alpha)$  following the type of range model used in the data.

nonstationary noise variance, and either a nonstationary variance or range for the latent field. Since the range exhibits slower MCMC convergence than the marginal variance, a “one-size-fits-most” approach would be to model heteroskedasticity both in the noise and in the latent field except when one suspects local anisotropy in the latent field. In the latter case, we advise against adding nonstationary variance of the latent field.

## 5.2 Scientific data analysis

We worked on a normalized difference vegetation index (NDVI) data set drawn from [Zhang and Banerjee \(2022\)](#), featuring over one million observations that exhibit anisotropy and also indicate spatially-varying (heteroskedastic) noise. We tested several models combining homoskedastic and heteroskedastic noise in (11)(e); and stationary and nonstationary, isotropic and anisotropic latent field as in (11)(c). The effective dimension of the data set



(a) Data with stationary isotropic range ( $\log(\gamma_A) = \text{diag}(0, 0, 0)$ ). (b) Data with nonstationary locally isotropic range ( $\log(\gamma_A) = \text{diag}(1, 0, 0)$ ). (c) Data with nonstationary locally isotropic range ( $\log(\gamma_A) = \text{diag}(1, 1, 1)$ ).

Figure 3: MCMC samples of the diagonal coefficients of the range PP log-variance parameter  $\log(\gamma_A)$ , following the type of range model used in the data.

was reduced through rounding of coordinates: the model was trained on 925,119 observations on 97,294 distinct locations since several locations had multiple observations mapped to them after the rounding of coordinates. This reduction in the latent field’s dimension allows, similarly to triangulation of the spatial domain (Lindgren et al., 2011) allows more elaborate analysis while retaining all observations. The remaining  $\sim 10\%$  of the observations (spatially spread using a max-min heuristic) were used for validation. We executed an NNGP with 10 neighbors and the max-min ordering with smoothness parameter  $\nu = 1.5$ . The nonstationary parameters were modeled using spatial effects as in equations (11)(e) and (11)(f), specified through predictive processes with Matérn smoothness 1.5 and range 0.2 with 50 knots. We also implemented an INLA-SPDE algorithm (Rue and Held, 2005; Lindgren and Rue, 2015; Bakka et al., 2019) as a benchmark, although the open version of R-INLA cannot model anisotropy (see, e.g., Fuglstad et al., 2015a, for some internal version implementations). Table 1 synthesizes the performances of the runs.

method	aniso.	nonstat.	heterosk.	DIC	train log-dens	pred. log-dens	min ESS	n. iter.	time (mn)	machine
NNGP	Yes	Yes	Yes	-25845	0.03	-0.20	87	1500	1498	Pyrene
NNGP	Yes	No	Yes	-18862	0.03	-0.23	68	1500	1526	Pyrene
NNGP	Yes	No	No	259491	-0.11	-0.35	97	1000	989	Pyrene
NNGP	No	No	Yes	-15707	0.03	-0.31	49	1000	192	Pyrene
NNGP	No	No	No	262442	-0.11	-0.41	92	1000	177	Pyrene
INLA	No	No	No	255804	cpo= -0.14				11	Helios

Table 1: Model comparisons for the NDVI analysis. For example, the second line refers to inference from an NNGP model with a stationary but anisotropic latent field range, and heteroskedastic noise variance. Other rows are similarly defined.

All NNGP runs were executed on the Pyrene computation cluster (32 threads and 64 GB RAM). Their MCMC convergence was monitored using univariate Gelman-Rubin-Brooks diagnostics (Gelman et al., 1992; Brooks and Gelman, 1998) and Effective Sample Sizes (ESS) for the high-level parameters (all the parameters of the models except the latent field  $w(\mathcal{S})$ ). Table 1 presents the minimum ESS. The number of iterations ranged between 1000 and 1500, incurring an effective running time ranging from two to sixteen hours depending upon the specific covariance structure in use. For software compatibility reasons, the INLA runs were done on an Acer Predator Helios laptop, with 12 threads, 32 GB RAM and 100 GB swap. In spite of its lower number of threads, the laptop is no slower than a cluster node. While the stationary INLA delivered, as expected, very expeditious output, it struggled with the nonstationary models and was unable to deliver even after 24 hours with the exhaustion of the 132 GB of RAM and swap. This, too, is not unexpected and can be attributed to the larger number of hyper-parameters in our models. To summarize, INLA outperforms our proposed MCMC-based implementation in stationary and isotropic settings, while our method is a much more viable option for nonstationary modeling with

complex covariance patterns (e.g., accommodating anisotropy and heterokedastic noise).

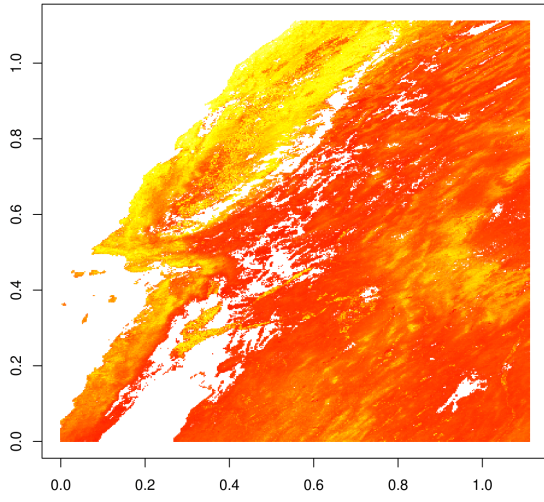
The models are compared using the DIC, the mean log-density of the observations, and the mean log-density of the predictions in Table 1. Nonstationary noise clearly boosts the model’s performance. The improvement brought by the elliptic covariance is more subdued, but the first three rows reveal that introducing more complexity in the anisotropy of models that are equivalent in every other aspect improves the DIC and the predicted log-density. The DIC of the INLA-fit model is coherent with the remainder of the non-heteroskedastic DICs. As for the validation score, it is computed with a leave-one-out log-density score. This method removes one observation of a spatial site, leaving the rest of the observations in the same spatial site, resulting in values between the smoothing and prediction scores. The nonstationary anisotropic model is also able to recover the spatially varying range and anisotropy of the observed data. Figure 4 summarizes the results from the full nonstationary model. Its first component, Figure 4(a) presents the raw observations. Figure 4(b) depicts the mean ellipses along with the mean latent field and shows that the ellipses fit the rays of the top-right corner, while they turn into small circles in the rougher left-hand side. The ellipses are inflated in the smoother regions reflecting increased range. Figure 4(c) maps the mean log variance of the noise revealing that the fuzzier left-hand side of the map is predicted with significantly more noise than the rest. Finally, Figure 4(d) presents the logarithm of the standard deviation of the summed latent field and fixed effects. The clearer dots correspond to locations left out for validation that incurred higher variance. Predictive variance and smoothing are clearly impacted by the covariance parameters and, in particular, by the noise variance. A final interesting observation is that the PP variance of the nonstationary range takes smaller values for the anisotropy components than for the determinant component. This is quite coherent with the map of the response variable 4(a):

we can see that there is an overall bottom left to top right anisotropy with little deviation, while the correlation range itself varies much more between, for example, the calm region of the center and the more troubled region on the upper left corner.

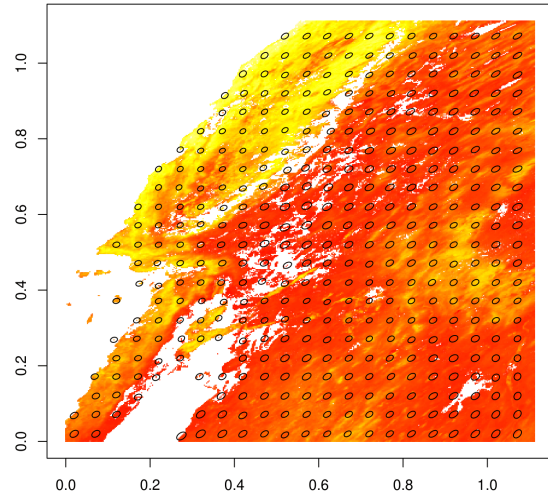
## 6 Summary and future directions

We have developed a class of hierarchical nonstationary NNGP models that overcome the bottlenecks of computational costs while offering nonstationary behavior through space-varying parameters in the spatial covariance kernel. We derive and exploit a closed form of the derivatives of the NNGP density with respect to spatially-indexed covariance parameters. These derivatives can also be used in HMC, MAP or other maximum likelihood approaches. The sparsity of NNGP factors along with dimension reduction using low-rank processes will allow scaling up the analysis to data sets with  $\sim 10^7+$  locations. Despite the challenges of complex scientific data sets, we have shown that nested AS-IS is a viable strategy for multi-layered hierarchical models with large data augmentations. Regardless of linking environmental predictors and spatial basis functions to the covariance structure, further investigation on the behavior of the matrix-log GP model is warranted.

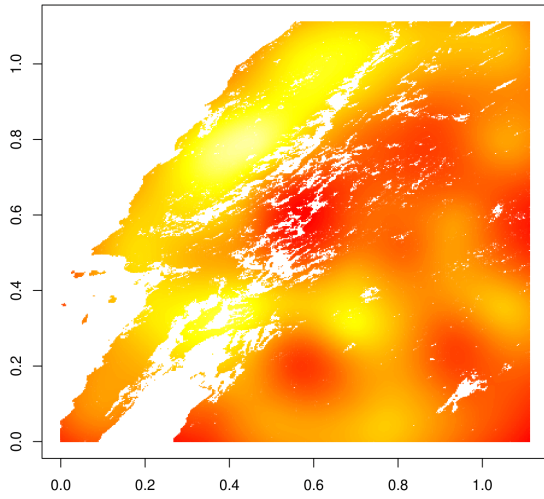
The proposed approach is applicable to any stationary kernel and should be explored beyond the Matérn kernels. Another possible extension is modeling in more than two dimensions. In particular, elliptic covariances in 3 dimensions may prove useful to quantify drifts such as rainfall moving across a territory. Ellipses in higher dimensions incur further differentiation, since the matrix logarithm of the range parameters will have 6 coordinates instead of 3. A computational scale up may be necessary. Given that we have derived the gradients of the model density, implementing *Maximum A Posteriori* (MAP) estimation is straightforward. Here, a key observation is that the high-level parameters appear to



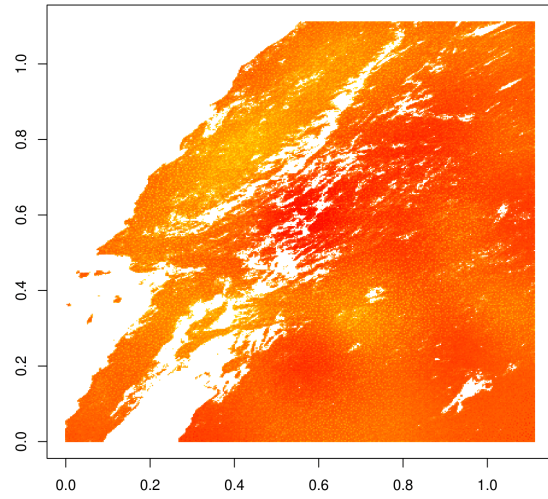
(a) Observed NDVI



(b) Predicted mean latent field and mean ellipses



(c) Predicted mean log-noise variance



(d) Log st-deviation of the predicted latent field

Figure 4: Maps generated using the nonstationary anisotropic, heteroskedastic model on the NDVI data set.

have unimodal distributions. The MAP could be attained by adapting the Gibbs sampler presented here into a coordinate descent algorithm. While an empirical Bayes approach would likely suffice for applications such as prediction of the response variable or smoothing, finding credible intervals around the MAP can present challenges. The computational effort in flops and RAM saved from MCMC can be reallocated to implementing NNGP models with richer variants of Vecchia’s approximation [Katzfuss et al. \(2020\)](#). Finally, while the approach is applicable to non-Gaussian data by modeling the data using exponential families, further investigations in these lines are needed to evaluate the effectiveness of estimating weakly identifiable parameters.

## References

- Bakka, H., Vanhatalo, J., Illian, J. B., Simpson, D., and Rue, H. (2019). Non-stationary gaussian models with physical barriers. *Spatial Statistics*, 29:268–288.
- Banerjee, S., Carlin, B. P., and Gelfand, A. E. (2014). *Hierarchical modeling and analysis for spatial data*. CRC press.
- Banerjee, S., Gelfand, A. E., Finley, A. O., and Sang, H. (2008). Gaussian predictive process models for large spatial data sets. *Journal of the Royal Statistical Society: Series B (Statistical Methodology)*, 70(4):825–848.
- Brooks, S. P. and Gelman, A. (1998). General methods for monitoring convergence of iterative simulations. *Journal of computational and graphical statistics*, 7(4):434–455.
- Coube-Sisqueille, S. (2021). *MCMC algorithms and hierarchical architectures for spatial modeling using Nearest Neighbor Gaussian Processes*. PhD thesis, Université de Pau et des Pays de l’Adour.

- Coube-Sisqueille, S. and Liquet, B. (2021). Improving performances of mcmc for nearest neighbor gaussian process models with full data augmentation. *Computational Statistics & Data Analysis*, page 107368.
- Cressie, N. and Johannesson, G. (2008). Fixed rank kriging for very large spatial data sets. *Journal of the Royal Statistical Society: Series B (Statistical Methodology)*, 70(1):209–226.
- Cressie, N. and Wikle, C. K. (2015). *Statistics for spatio-temporal data*. John Wiley & Sons.
- Datta, A., Banerjee, S., Finley, A. O., and Gelfand, A. E. (2016). Hierarchical nearest-neighbor gaussian process models for large geostatistical datasets. *Journal of the American Statistical Association*, 111(514):800–812.
- Filippone, M., Zhong, M., and Girolami, M. (2013). A comparative evaluation of stochastic-based inference methods for gaussian process models. *Machine Learning*, 93(1):93–114.
- Finley, A. O., Datta, A., Cook, B. D., Morton, D. C., Andersen, H. E., and Banerjee, S. (2019). Efficient algorithms for bayesian nearest neighbor gaussian processes. *Journal of Computational and Graphical Statistics*, 28(2):401–414.
- Fuentes, M. (2002). Spectral methods for nonstationary spatial processes. *Biometrika*, 89(1):197–210.
- Fuglstad, G.-A., Simpson, D., Lindgren, F., and Rue, H. (2015a). Does non-stationary spatial data always require non-stationary random fields? *Spatial Statistics*, 14:505–531.
- Fuglstad, G.-A., Simpson, D., Lindgren, F., and Rue, H. (2015b). Interpretable priors for hyperparameters for gaussian random fields. *arXiv preprint arXiv:1503.00256*.

- Gelfand, A. E., Diggle, P., Guttorp, P., and Fuentes, M. (2010). *Handbook of Spatial Statistics (Chapman & Hall CRC Handbooks of Modern Statistical Methods)*. Chapman & Hall CRC Handbooks of Modern Statistical Methods. Taylor and Francis.
- Gelfand, A. E., Fuentes, M., Hoeting, J. A., and Smith, R. L. (2019). *Handbook of environmental and ecological statistics*. CRC Press.
- Gelman, A., Rubin, D. B., et al. (1992). Inference from iterative simulation using multiple sequences. *Statistical science*, 7(4):457–472.
- Guhaniyogi, R., Finley, A. O., Banerjee, S., and Gelfand, A. E. (2011). Adaptive gaussian predictive process models for large spatial datasets. *Environmetrics*, 22(8):997–1007.
- Guhaniyogi, R., Finley, A. O., Banerjee, S., and Kobe, R. K. (2013). Modeling complex spatial dependencies: Low-rank spatially varying cross-covariances with application to soil nutrient data. *Journal of Agricultural, Biological and Environmental Statistics*, 18:274–298.
- Guinness (2018). Permutation and grouping methods for sharpening gaussian process approximations. *Technometrics*, 60(4):415–429.
- Heaton, M. J., Datta, A., Finley, A. O., Furrer, R., Guinness, J., Guhaniyogi, R., Gerber, F., Gramacy, R. B., Hammerling, D., Katzfuss, M., et al. (2019). A case study competition among methods for analyzing large spatial data. *Journal of Agricultural, Biological and Environmental Statistics*, 24(3):398–425.
- Heinonen, M., Mannerström, H., Rousu, J., Kaski, S., and Lähdesmäki, H. (2016). Non-stationary gaussian process regression with hamiltonian monte carlo. In *Artificial Intelligence and Statistics*, pages 732–740.

- Hengl, T. (2009). A practical guide to geostatistical mapping.
- Higdon, D. (1998). A process-convolution approach to modelling temperatures in the north atlantic ocean. *Environmental and Ecological Statistics*, 5(2):173–190.
- Ingebrigtsen, R., Lindgren, F., Steinsland, I., and Martino, S. (2015). Estimation of a non-stationary model for annual precipitation in southern norway using replicates of the spatial field. *Spatial Statistics*, 14:338–364.
- Katzfuss, M. and Guinness, J. (2021). A general framework for vecchia approximations of gaussian processes. *Statistical Science*, 36(1):124–141.
- Katzfuss, M., Guinness, J., Gong, W., and Zilber, D. (2020). Vecchia approximations of gaussian-process predictions. *Journal of Agricultural, Biological and Environmental Statistics*, 25(3):383–414.
- Kleiber, W. and Nychka, D. (2012). Nonstationary modeling for multivariate spatial processes. *Journal of Multivariate Analysis*, 112:76–91.
- Knorr-Held, L. and Rue, H. (2002). On block updating in markov random field models for disease mapping. *Scandinavian Journal of Statistics*, 29(4):597–614.
- Lemos, R. T., Sansó, B., Higdon, D., Mendelssohn, R., Wikle, C. K., Milliff, R. F., Lemos, R. T., and Sansó, B. (2009). A spatio-temporal model for mean, anomaly, and trend fields of north atlantic sea surface temperature [with comments]. *Journal of the American Statistical Association*, 104(485):5–25.
- Lindgren, F. and Rue, H. (2015). Bayesian Spatial Modelling with *R* - **INLA**. *Journal of Statistical Software*, 63(19).

- Lindgren, F., Rue, H., and Lindström, J. (2011). An explicit link between gaussian fields and gaussian markov random fields: the stochastic partial differential equation approach. *Journal of the Royal Statistical Society: Series B (Statistical Methodology)*, 73(4):423–498.
- Neal, R. M. et al. (2011). Mcmc using hamiltonian dynamics. *Handbook of markov chain monte carlo*, 2(11):2.
- Paciorek, C. J. (2003). *Nonstationary Gaussian processes for regression and spatial modeling*. PhD thesis, Citeseer.
- Pourahmadi, M. (1999). Joint mean-covariance models with applications to longitudinal data: unconstrained parameterisation. *Biometrika*, 86(3):677–690.
- Pourahmadi, M. (2007). Cholesky Decompositions and Estimation of A Covariance Matrix: Orthogonality of Variance–Correlation Parameters. *Biometrika*, 94(4):1006–1013.
- Risser, M. D. (2016). Nonstationary spatial modeling, with emphasis on process convolution and covariate-driven approaches. *arXiv preprint arXiv:1610.02447*.
- Risser, M. D. and Calder, C. A. (2015). Regression-based covariance functions for nonstationary spatial modeling. *Environmetrics*, 26(4):284–297.
- Rue, H. and Held, L. (2005). *Gaussian Markov random fields: theory and applications*. Monographs on statistics and applied probability 104. Chapman & Hall/CRC, 1 edition.
- Spiegelhalter, D. J., Best, N. G., Carlin, B. P., and Van der Linde, A. (1998). Bayesian deviance, the effective number of parameters, and the comparison of arbitrarily complex models. Technical report, Research Report, 98-009.

- Stein, M. L. (1999). *Interpolation of Spatial Data: Some Theory for Kriging*. Springer Series in Statistics. Springer-Verlag New York, 1 edition.
- Stein, M. L., Chi, Z., and Welty, L. J. (2004). Approximating likelihoods for large spatial data sets. *Journal of the Royal Statistical Society: Series B (Statistical Methodology)*, 66(2):275–296.
- Tang, W., Zhang, L., and Banerjee, S. (2021). On identifiability and consistency of the nugget in gaussian spatial process models. *Journal of the Royal Statistical Society: Series B (Statistical Methodology)*, 83(5):1044–1070.
- Vecchia, A. V. (1988). Estimation and model identification for continuous spatial processes. *Journal of the Royal Statistical Society: Series B (Methodological)*, 50(2):297–312.
- Yang, H.-C. and Bradley, J. R. (2021). Bayesian inference for big spatial data using non-stationary spectral simulation. *Spatial Statistics*, 43:100507.
- Yu, Y. and Meng, X.-L. (2011). To center or not to center: That is not the question—an ancillarity–sufficiency interweaving strategy (asis) for boosting mcmc efficiency. *Journal of Computational and Graphical Statistics*, 20(3):531–570.
- Zhang, H. (2004). Inconsistent estimation and asymptotically equal interpolations in model-based geostatistics. *Journal of the American Statistical Association*, 99(465):250–261.
- Zhang, L. and Banerjee, S. (2022). Spatial factor modeling: A bayesian matrix-normal approach for misaligned data. *Biometrics*, 78(2):560–573.

# Supplement to “Nonstationary Spatial Process Models with Spatially Varying Covariance Kernels”

## S1 Some results on the nonstationary NNGP

### S1.1 Recursive conditional form of nonstationary NNGP

We begin with the conditional density on the left hand side of (8) and proceed as below:

$$\begin{aligned} \tilde{f}(w(s_i) | w(\mathcal{S}_{i-1}), \theta(\mathcal{S})) &= f(w(s_i) | w(pa(s_i)), \theta(\mathcal{S})) \\ &= f(w(s_i \cup pa(s_i)) | \theta(\mathcal{S})) / f(w(pa(s_i)) | \theta(\mathcal{S})). \end{aligned} \quad (\text{S1})$$

The joint distributions  $f(w(s_i \cup pa(s_i)) | \theta(\mathcal{S}))$  and  $f(w(pa(s_i)) | \theta(\mathcal{S}))$  are fully specified by  $\Sigma(s_i \cup pa(s_i), \theta(\mathcal{S}))$  and  $\Sigma(pa(s_i), \theta(\mathcal{S}))$ . Since the covariance functions given by (5) or (6) specify  $\Sigma(s_i, s_j)$  using only  $\{\theta(s_i), \theta(s_j)\}$  instead of  $\theta(\mathcal{S})$ , we obtain  $f(w(s_i \cup pa(s_i)) | \theta(\mathcal{S})) = f(w(s_i \cup pa(s_i)) | \theta(s_i \cup pa(s_i)))$  and  $f(w(pa(s_i)) | \theta(\mathcal{S})) = f(w(pa(s_i)) | \theta(pa(s_i)))$ , which is equal to  $f(w(pa(s_i)) | \theta(s_i \cup pa(s_i)))$  since  $w(pa(s_i))$  is conditionally independent of  $\theta(s_i)$  given  $\theta(pa(s_i))$ . Substituting these expressions into the right hand side of (S1) yields (8).

### S1.2 Marginal variance of nonstationary NNGP

Let  $\Sigma(\mathcal{S}) = (K(s_i, s_j))$  and let  $\Sigma_0(\mathcal{S}) = (K_0(s_i, s_j))$  be the spatial covariance and correlation matrices, respectively, constructed from the nonstationary covariance function  $K(s_i, s_j)$  and the corresponding correlation function  $K_0(s_i, s_j)$ . Let  $\tilde{\Sigma}(\mathcal{S})^{-1} = \tilde{R}^\top \tilde{R}$  be the NNGP precision matrix using the nonstationary covariance  $K(\cdot)$ , where  $\tilde{R}$  is the NNGP factor of  $\tilde{\Sigma}(\mathcal{S})^{-1}$ . Analogously, let  $\tilde{R}_0$  be the NNGP precision matrix using the nonstationary correlation  $\Sigma_0$  from (4) and either (5) or (6). If  $\bar{\sigma}_i = \sqrt{\text{var}(w(s_i) | w(pa(s_i)))}$ , then a standard expression is

$\bar{\sigma}_i = (\Sigma(s_i, s_i) - \Sigma(s_i, pa(s_i))\Sigma(pa(s_i), pa(s_i))^{-1}\Sigma(pa(s_i), s_i))^{1/2}$ . Therefore, the  $i$ -th row of  $\tilde{R}$  comprises (i)  $1/\bar{\sigma}_i$  at index  $i$ ; (ii)  $-\Sigma(s_i, pa(s_i))\Sigma(pa(s_i), pa(s_i))^{-1}/\bar{\sigma}_i$  at indices corresponding to  $pa(s_i)$ ; and (iii) 0 elsewhere. Letting  $\bar{\sigma}_{0i}$  be the conditional correlation obtained from  $\Sigma_0$  instead of  $\Sigma$ , it is easily seen that  $\bar{\sigma}_i = \sigma(s_i)(\bar{\sigma}_{0i})$  using the elementary observations that  $\sigma(s_i)^2 = \Sigma(s_i, s_i)$  (by definition of  $\sigma(s_i)$ ) and that  $\Sigma(\mathcal{A}, \mathcal{B}) = \text{diag}(\sigma(\mathcal{A}))\Sigma_0(\mathcal{A}, \mathcal{B})\text{diag}(\sigma(\mathcal{B}))$ , where  $\mathcal{A}$  and  $\mathcal{B}$  are any two non-empty subsets of  $\mathcal{S}$ . Thus,

$$\begin{aligned}\bar{\sigma}_i &= (\Sigma(s_i, s_i) - \Sigma(s_i, pa(s_i))\Sigma(pa(s_i), pa(s_i))^{-1}\Sigma(pa(s_i), s_i))^{1/2} \\ &= \sigma(s_i) (\Sigma_0(s_i, s_i) - \Sigma_0(s_i, pa(s_i))\Sigma_0(pa(s_i), pa(s_i))^{-1}\Sigma_0(pa(s_i), s_i))^{1/2} \quad (\text{S2}) \\ &= \sigma(s_i)(\bar{\sigma}_{0i})\end{aligned}$$

Using this relationship, we can express the coefficients of row  $i$  in  $\tilde{R}$  as (i)  $1/(\bar{\sigma}_{0i})\sigma(s_i)$  at position  $i$ ; (ii)  $(-\Sigma_0(s_i, pa(s_i))\Sigma_0(pa(s_i), pa(s_i))^{-1}/(\bar{\sigma}_{0i})) = \tilde{R}_0(i, pa(i))\text{diag}(\sigma(pa(s_i)))^{-1}$  at the indices corresponding to  $pa(s_i)$ , which means that  $\tilde{R}(i, j) = \tilde{R}_0(i, j)/\sigma(s_j)$  for all  $s_j \in pa(s_i)$ ; and (iii) 0 elsewhere. Comparing elements we obtain  $\tilde{R} = \tilde{R}_0\text{diag}(\sigma(\mathcal{S}))^{-1}$ .

## S2 KL divergence between nonstationary NNGP and full nonstationary GP

### S2.1 Spatially indexed variances

The Kullback-Leibler (KL) divergence between two multivariate normal distributions  $\mathcal{N}(\mu_1, \Sigma_1)$  and  $\mathcal{N}(\mu_2, \Sigma_2)$  is

$$KL(\mathcal{N}_1 \parallel \mathcal{N}_2) = \frac{1}{2} \left( \text{tr}(\Sigma_2^{-1}\Sigma_1) + (\mu_2 - \mu_1)^\top \Sigma_2^{-1}(\mu_2 - \mu_1) - k + \ln \left( \frac{|\Sigma_2|}{|\Sigma_1|} \right) \right).$$

Recalling that the NNGP precision is given by  $\tilde{\Sigma}(\mathcal{S})^{-1} = \text{diag}(\sigma(\mathcal{S}))^{-1}(\tilde{R}_0^\top \tilde{R}_0)\text{diag}(\sigma(\mathcal{S}))^{-1}$ , that the full GP's covariance matrix is  $\text{diag}(\sigma(\mathcal{S}))\Sigma_0\text{diag}(\sigma(\mathcal{S}))$ , and that the NNGP and

GP mean are equal, the KL divergence between a nonstationary full GP with zero mean and the NNGP is  $\frac{1}{2} \text{tr} \left( \Sigma_0 \tilde{R}_0^T \tilde{R}_0 \right) + \ln \left( \frac{|\tilde{R}_0^T \tilde{R}_0|}{|\Sigma_0|} \right)$ , which is the KL divergence between  $N(0, \Sigma_0)$  and  $N(0, \tilde{\Sigma}_0)$ . It follows that spatially indexed variances do not affect the KL divergence between nonstationary full GPs and NNGPs.

## S2.2 Spatially indexed variances and scalar ranges

Synthetic data sets with 2500 observations were simulated on a domain with size  $5 \times 5$ . The spatially variable log-range had mean  $\log(0, 05)$ . Three factors were tested:

- the intensity of nonstationarity, by letting the log range’s variance take different values (0.1, 0.3, and 0.5).
- the ordering (coordinate, max-min, random, middleout).
- the number of parents (5, 10, 20).

Using a linear model with interactions shows that the most important factor is the number of parents. The NNGP approximation can be further improved using the max-min and random order, joining [Guinness \(2018\)](#)’s conclusions for stationary models in 2 dimensions. The intensity of the nonstationarity plays a small role. See table S1 for more details about the effects of the factors.

Table S1: Summary of linear regression of the KL divergence, in the scalar range case.

The reference case has coordinate ordering, 5 nearest neighbours, and a log-range variance of 0.05

	Estimate	Std. Error	t value	Pr(>  t )
(Intercept)	41.08	0.71	58.09	0.00
nonstat.intensity 0.3	2.56	0.46	5.53	0.00
nonstat.intensity 0.5	5.39	0.46	11.65	0.00
ordering max min	-4.18	0.93	-4.51	0.00
ordering middle out	-1.90	0.93	-2.06	0.04
ordering random	-4.34	0.93	-4.69	0.00
10 nearest neighbours	-31.59	0.93	-34.12	0.00
20 nearest neighbours	-41.27	0.93	-44.58	0.00
max min: 10	0.83	1.31	0.63	0.53
middle out: 10	0.42	1.31	0.32	0.75
random: 10	0.99	1.31	0.76	0.45
max min: 20	3.19	1.31	2.43	0.02
middle out: 20	1.24	1.31	0.94	0.35
random: 20	3.35	1.31	2.56	0.01

### S2.3 Elliptic range case

Synthetic data sets with 2500 observations were simulated on a domain with size  $5 \times 5$ . The spatially variable log-matrix range had mean  $\log(0.05)$ . Three factors were tested:

- the intensity of nonstationarity, by letting the variance of the coordinates of the log-range matrix take different values:  $(0.1 \times I_3, 0.3 \times I_3, \text{ and } 0.5 \times I_3)$ .
- the ordering (coordinate, max-min, random, middleout).
- the number of parents (5, 10, 20).

The conclusion we draw from table S2 are the same as before.

Table S2: Summary of linear regression of the KL divergence, in the elliptic range case.

The reference case has coordinate ordering, 5 nearest neighbours, and a log-range variance of 0.05

	Estimate	Std. Error	t value	Pr(>  t )
(Intercept)	41.08	0.71	58.09	0.00
nonstat.intensity 0.3	2.56	0.46	5.53	0.00
nonstat.intensity 0.5	5.39	0.46	11.65	0.00
ordering max min	-4.18	0.93	-4.51	0.00
ordering middle out	-1.90	0.93	-2.06	0.04
ordering random	-4.34	0.93	-4.69	0.00
10 nearest neighbours	-31.59	0.93	-34.12	0.00
20 nearest neighbours	-41.27	0.93	-44.58	0.00
max min: 10	0.83	1.31	0.63	0.53
middle out: 10	0.42	1.31	0.32	0.75
random: 10	0.99	1.31	0.76	0.45
max min: 20	3.19	1.31	2.43	0.02
middle out: 20	1.24	1.31	0.94	0.35
random: 20	3.35	1.31	2.56	0.01

## S3 Details about Interweaving

### S3.1 Interweaving

Interweaving is a method introduced by [Yu and Meng \(2011\)](#), which improves the mixing of models relying on data augmentation. Rather than finding a parametrization that ”works well”, this method exploits the discrepancy between two parametrizations of the latent field. Usually various parametrizations of the data augmentation are available. For example, in the context of our NNGP model, the latent field

$$w \stackrel{a \text{ priori}}{\sim} \mathcal{N}(0, \tilde{\Sigma})$$

with  $\tilde{\Sigma} = (\tilde{R}^T \tilde{R})^{-1}$  can be re-parametrized as

$$w^* = \tilde{R}w \stackrel{a \text{ priori}}{\sim} \mathcal{N}(0, I_n).$$

The component-wise Interweaving strategy of [Yu and Meng \(2011\)](#) can be applied when two data augmentations  $w_1$  and  $w_2$  have a joint distribution  $[\theta, w_1, w_2]$  (even if it is degenerate) such that its marginals  $[\theta, w_1]$  and  $[\theta, w_2]$  correspond to the two models with the different data augmentations. It takes advantage of the discordance between the two parametrizations to construct the following step in order to sample  $\theta^{t+1}$ :

$$[\theta, w_2' | w_1^t, \dots] \rightarrow [\theta^{t+1}, w_1^{t+0.5} | w_2', \dots],$$

“...” being the other parameters of the model. Since all the draws are done from full conditional distributions, the target joint distribution is preserved. Joint sampling of the parameter and the data augmentation is much easier to implement when decomposed as:

$$\underbrace{[\theta | w_1^t, \dots] \rightarrow [w_2' | w_1^t, \theta, \dots]}_{[\theta, w_2' | w_1^t, \dots]} \rightarrow \underbrace{[\theta^{t+1} | w_2', \dots] \rightarrow [w_1^{t+0.5} | w_2', \theta^{t+1}, \dots]}_{[\theta^{t+1}, w_1^{t+0.5} | w_2', \dots]}.$$

It is possible that the joint distribution is degenerate as long as it is well-defined, so that  $[w_2' | \theta, w_1^t]$  and  $[w_1^{t+0.5} | w_2', \theta^{t+1}, \dots]$  are often deterministic transformations (in our application they are). For this reason even though the data augmentation is changed at the end of the sampling of  $\theta$ ,  $w$  still has to be updated in a separate step in order to have an irreducible chain: that is why we indexed it by  $t + 0.5$ .

The method builds its efficiency upon the fact that the parameter  $\theta$  sampled in the first step,  $[\theta, w_2' | w_1^t, \dots]$ , is not used later in the algorithm. This first step is therefore equivalent to  $[w_2' | w_1^t, \dots]$ . If there is little correlation between the two parametrizations  $w_1$  and  $w_2$ , the subsequent draw  $[\theta^{t+1} | w_2', \dots]$  can produce a new parameter  $\theta^{t+1}$  far from  $\theta^t$  even if there is

a strong correlation between  $\theta$  and both  $w_1$  and  $w_2$ . It is not an alternating scheme, that requires at  $\theta$  to have a weak bond with at least either  $w_1$  and  $w_2$ .

The strategy being based on the discordance between two parametrizations, it is a good choice to pick an ancillary-sufficient couple, giving an Ancillary-Sufficient Interweaving Strategy (AS-IS). Following the terminology of [Yu and Meng \(2011\)](#),  $w$  is sufficient when *a posteriori*  $(\theta|w, z) = (\theta|w)$ ,  $z$  being the observed data and  $\theta$  being the target high-level parameter. It is sufficient when it is *a priori* independent from  $\theta$ . AS-IS has been shown to be effective for GP models: [Filippone et al. \(2013\)](#) show empirically that updating covariance parameters in a Gaussian Process model benefits from Interweaving the natural parametrization  $w$  (sufficient) and the whitened parametrization  $w^*$  (ancillary), while [Coube-Sisqueille and Liquet \(2021\)](#) use centred and non-centred parametrizations to sample efficiently the coefficients associated with the fixed effects.

### S3.2 Nested Interweaving for high-level parameters

The problem in our case is that there are latent fields on various layers of the hierarchical model. Nested AS-IS is envisioned by [Yu and Meng \(2011\)](#) for such configurations, even though the authors do not provide application to realistic models.

Consider a high-level parameter concerning the log-GP distributions of the covariance parameters,  $\gamma_\theta$  or  $\gamma_\tau$  from(11). This parameter is noted  $\gamma$ . Note  $\tilde{W}$  the sufficient parametrization and  $\tilde{W}^*$  the ancillary parametrization for the corresponding log-GP field of covariance parameters. In the case of anisotropic range,  $\tilde{W}^* = chol(\gamma_A \otimes I_p)^{-1}\tilde{W}$ . In all other cases,  $\tilde{W}^* = \tilde{W}/\sqrt{\gamma}$ . Those parametrizations form a sufficient-ancillary pair, and can be a natural (sufficient) and whitened (ancillary) couple when we are working with marginal variance parameters ([Filippone et al., 2013](#)), or a centered (sufficient) and natural (ancillary) pair when working with the regression coefficients ([Coube-Sisqueille and Liquet, 2021](#)). Eventually, note  $w$  and  $w^*$  the respectively natural and whitened parametrizations of the NNGP latent

field from (12)(a).

A nested Interweaving step aiming to update  $\gamma$  can be devised as

$$\begin{array}{c}
 [\gamma, \tilde{W}^*, w^* | \tilde{W}, w, \dots] \rightarrow [\gamma, \tilde{W}, w^* | \tilde{W}^*, w, \dots] \\
 \swarrow \\
 [\gamma, \tilde{W}^*, w | \tilde{W}, w^*, \dots] \rightarrow [\gamma, \tilde{W}, w | \tilde{W}^*, w^*, \dots]
 \end{array}
 \left. \vphantom{\begin{array}{c} \\ \\ \end{array}} \right\} \text{Interweaving } w \tag{S3}$$

Interweaving  $W$

Like before, it is much easier to sample sequentially, for example the blocked draw

$[\gamma, \tilde{W}^*, w^* | \tilde{W}, w, \dots]$  writes as

$$[\gamma | \tilde{W}, w, \dots] \rightarrow \underbrace{[\tilde{W}^* | \gamma, \tilde{W}, w, \dots]}_{\text{deterministic}} \rightarrow \underbrace{[w^* | \gamma, \tilde{W}, \tilde{W}^*, w, \dots]}_{\text{deterministic}}.$$

### S3.3 Layout of the MCMC algorithm

1. Block update of the latent field using [Datta et al. \(2016\)](#), Section 4.1. For  $\mathcal{S}_1, \dots, \mathcal{S}_k$  such that  $\mathcal{S}_1 \cup \dots \cup \mathcal{S}_k = \mathcal{S}$ , draw

$$[w(\mathcal{S}_1) | w(\mathcal{S} \setminus \mathcal{S}_1), \beta, \theta, \tau, X, z] \rightarrow \dots \rightarrow [w(\mathcal{S}_k) | w(\mathcal{S} \setminus \mathcal{S}_k), \beta, \theta, \tau, X, z].$$

2. Interweaving update of  $\beta$  using [Coube-Sisquille and Liquet \(2021\)](#), Section 2.

$$\underbrace{[\beta | w, \tau]}_{\text{ancillary}} \rightarrow \underbrace{[w_{\text{center}} | w, \beta]}_{\text{deterministic}} \rightarrow \underbrace{[\beta | w_{\text{center}}, \theta]}_{\text{sufficient}} \rightarrow \underbrace{[w | w_{\text{center}}, \beta]}_{\text{deterministic}}$$

3. Joint HMC-within-Gibbs update of  $\tilde{W}_\tau$  and  $\beta_\tau$ .

$$[\beta_\tau, \tilde{W}_\tau | w, \beta, \gamma_\tau]$$

4. Interweaving update of  $\gamma_\tau$ . This low-dimension parameter can be sampled with HMC or random-walk metropolis.

$$\underbrace{[\gamma_\tau | \tilde{W}_\tau]}_{\text{sufficient}} \rightarrow \underbrace{[\tilde{W}_\tau^* | \gamma_\tau, \tilde{W}_\tau]}_{\text{deterministic}} \rightarrow \underbrace{[\gamma_\tau | \tilde{W}_\tau^*, \beta_\tau, w, \beta]}_{\text{ancillary}} \rightarrow \underbrace{[\tilde{W}_\tau | \gamma_\tau, \tilde{W}_\tau^*]}_{\text{deterministic}}$$

5. HMC-within-interweaving update of the range parameters  $\tilde{W}_\alpha$  and  $\beta_\alpha$ .

$$\underbrace{[\tilde{W}_\alpha, \beta_\alpha | w, \gamma_\alpha]}_{\text{sufficient}} \rightarrow \underbrace{[w^* | w, \alpha]}_{\text{deterministic}} \rightarrow \underbrace{[\tilde{W}_\alpha, \beta_\alpha | w^*, \gamma_\alpha, \beta]}_{\text{ancillary}} \rightarrow \underbrace{[w | w^*, \alpha]}_{\text{deterministic}}$$

6. Nested Interweaving update of  $\gamma_\alpha$ . This low-dimension parameter can be sampled with HMC or random-walk metropolis.

$$\begin{array}{ccccccc} [\gamma_\alpha | \tilde{W}_\alpha] & \rightarrow & [\tilde{W}_\alpha^* | \gamma_\alpha, \tilde{W}_\alpha] & \rightarrow & [\gamma_\alpha | \tilde{W}_\alpha^*, w, \beta_\alpha, X_\alpha] & \rightarrow & [\tilde{W}_\alpha | \gamma_\alpha, \tilde{W}_\alpha^*] \rightarrow [w^* | w, \alpha] \\ \underbrace{\rightarrow [\gamma_\alpha | \tilde{W}_\alpha] \rightarrow [\tilde{W}_\alpha^* | \gamma_\alpha, \tilde{W}_\alpha] \rightarrow [\gamma_\alpha | \tilde{W}_\alpha^*, w^*, \beta_\alpha, X_\alpha, \beta, X, z] \rightarrow [\tilde{W}_\alpha | \gamma_\alpha, \tilde{W}_\alpha^*] \rightarrow [w | w^*, \alpha]}_{\text{Interweaving } \tilde{W}_\alpha} & & & & & & \end{array} \left. \vphantom{\begin{array}{ccccccc} \end{array}} \right\} \text{Interweaving } w$$

7. HMC-within-interweaving update of the marginal variance parameters  $\tilde{W}_\sigma$  and  $\beta_\sigma$ .

$$\underbrace{[\tilde{W}_\sigma, \beta_\sigma | w, \gamma_\sigma]}_{\text{sufficient}} \rightarrow \underbrace{[w^* | w, \sigma]}_{\text{deterministic}} \rightarrow \underbrace{[\tilde{W}_\sigma, \beta_\sigma | w^*, \gamma_\sigma, \beta]}_{\text{ancillary}} \rightarrow \underbrace{[w | w^*, \sigma]}_{\text{deterministic}}$$

8. Nested Interweaving update of  $\gamma_\sigma$ . This low-dimension parameter can be sampled with HMC or random-walk metropolis.

$$\begin{array}{ccccccc} [\gamma_\sigma | \tilde{W}_\sigma] & \rightarrow & [\tilde{W}_\sigma^* | \gamma_\sigma, \tilde{W}_\sigma] & \rightarrow & [\gamma_\sigma | \tilde{W}_\sigma^*, w, \beta_\sigma, X_\sigma] & \rightarrow & [\tilde{W}_\sigma | \gamma_\sigma, \tilde{W}_\sigma^*] \rightarrow [w^* | w, \sigma] \\ \underbrace{\rightarrow [\gamma_\sigma | \tilde{W}_\sigma] \rightarrow [\tilde{W}_\sigma^* | \gamma_\sigma, \tilde{W}_\sigma] \rightarrow [\gamma_\sigma | \tilde{W}_\sigma^*, w^*, \beta_\sigma, X_\sigma, \beta, X, z] \rightarrow [\tilde{W}_\sigma | \gamma_\sigma, \tilde{W}_\sigma^*] \rightarrow [w | w^*, \sigma]}_{\text{Interweaving } \tilde{W}_\sigma} & & & & & & \end{array} \left. \vphantom{\begin{array}{ccccccc} \end{array}} \right\} \text{Interweaving } w$$

## S4 Gradients for HMC updates of the covariance parameters

### S4.1 Gradient of the log-density of the observations with respect to the latent NNGP field.

A technical point to obtain the gradient of the log-density of the observations with respect to the latent field is that there can be several observations at the same spatial site. Consider a site  $s \in \mathcal{S}$ , and note these observations  $obs(s)$ . Note  $obs(s) = \{i/M_{i,j} = 1\}$  in (11) (a), that is the indices of the observations made at the spatial site  $s$ . We obtain, by virtue of the conditional independence of the observations of  $z$  in (11)(a),

$$\begin{aligned} \frac{\partial l(z|w(\mathcal{S}),\beta,\tau)}{\partial w(s)} &= \frac{\partial l(z_{obs(s)}|w(\mathcal{S}),\beta,\tau_{obs(s)})}{\partial w(s)} \\ &= \frac{\partial \sum_{x \in obs(s)} (z(x) - X(x)\beta - w(s))^2 / 2\tau(x)^2}{\partial w(s)} \\ &= \sum_{x \in obs(s)} (w(s) - (z(x) - X(x)\beta)) / \tau(x)^2, \end{aligned}$$

leading to the result.

### S4.2 Gradient with respect to $\log(\sigma^2)$

*Sufficient augmentation.* When sufficient augmentation is used, the marginal variance intervenes in the NNGP density of the latent field. The resulting gradient is

$$-\nabla_{\log(\sigma^2)} h^{sufficient}(\log(\sigma^2)) = (1/2, \dots, 1/2) - \sigma^{-1}(\mathcal{S}) \circ \left( \text{diag}(w) \tilde{R}_0^T \tilde{R}_0 \text{diag}(w) \quad \sigma^{-1}(\mathcal{S}) \right) / 2. \tag{S4}$$

We start from

$$h^{sufficient}(\log(\sigma^2)) = f(w(\mathcal{S})|\sigma^2(\mathcal{S})),$$

$\tilde{f}(\cdot)$  being the NNGP density from (11) (b). From (9), we write

$$\tilde{f}(w(\mathcal{S})|\sigma^2(\mathcal{S})) = \exp\left(-\sigma^{-1}(\mathcal{S})^T \text{diag}(w)\tilde{R}_0^T \tilde{R}_0 \text{diag}(w)\sigma^{-1}(\mathcal{S})/2\right) \prod_{i=1}^n (\tilde{R}_0)_{i,i}/\sigma(s_i).$$

Passing to the negated log-density

$$\begin{aligned} -\log\left(\tilde{f}(w(\mathcal{S})|\sigma^2(\mathcal{S}))\right) &= cst + \sum_{i=1}^n \log(\sigma(s_i)) + \\ &\quad \sigma^{-1}(\mathcal{S})^T \text{diag}(w)\tilde{R}_0^T \tilde{R}_0 \text{diag}(w)\sigma^{-1}(\mathcal{S})/2. \end{aligned}$$

On the one hand,

$$\nabla_{\log(\sigma^2)\Sigma_{i=1}^n \log(\sigma(s_i))} = \nabla_{\log(\sigma^2)\Sigma_{i=1}^n \log((\sigma^2(s_i))^{1/2})} = \nabla_{\log(\sigma^2)\Sigma_{i=1}^n \log(\sigma^2(s_i))/2} = (1/2, \dots, 1/2)$$

On the other hand, we can write the Jacobian of  $\sigma^{-1}$  with respect to  $\log(\sigma^2)$ :

$$J_{\log(\sigma^2)\sigma^{-1}}(\mathcal{S}) = J_{\log(\sigma^2)} \exp(-\log(\sigma^2)/2) = -\text{diag}(\sigma^{-1}(\mathcal{S})/2).$$

We also find the following gradient:

$$\nabla_{\sigma^{-1}\sigma^{-1}(\mathcal{S})^T \text{diag}(w)\tilde{R}_0^T \tilde{R}_0 \text{diag}(w)\sigma^{-1}(\mathcal{S})/2} = \text{diag}(w)\tilde{R}_0^T \tilde{R}_0 \text{diag}(w)\sigma^{-1}(\mathcal{S}).$$

With the Jacobian chain rule, we combine the two previous formulas to find

$$-\nabla_{\log(\sigma^2)\sigma^{-1}(\mathcal{S})^T \text{diag}(w)\tilde{R}_0^T \tilde{R}_0 \text{diag}(w)\sigma^{-1}(\mathcal{S})/2} = \sigma^{-1}(\mathcal{S}) \circ \left(\text{diag}(w)\tilde{R}_0^T \tilde{R}_0 \text{diag}(w)\sigma^{-1}(\mathcal{S})\right)/2,$$

with  $\circ$  denoting the Hadamard product. Combining both hands, we have the result.

*Ancillary augmentation.* When ancillary augmentation is used, the marginal variance has an impact on the observed field likelihood with respect to the latent field. The gradient writes

$$-\nabla_{W_\sigma} g_\sigma^{\text{ancillary}}(W_\sigma) = -\nabla_w l(z(\mathcal{S})|w, \beta, \tau) \circ (w/2), \quad (\text{S5})$$

◦ being the Hadamard product, and  $\nabla_{W_\sigma} l(z(\mathcal{S})|w(\mathcal{S}), \beta, \tau)$  being discussed in Section S4.1.

We start from

$$-g_\sigma^{\text{ancillary}}(W_\sigma) = -l(z|w(\mathcal{S}) = \tilde{R}^{-1}w^*(\mathcal{S}), \beta, \tau),$$

from (11) (a). The marginal variance affects the Gaussian density  $l(\cdot)$  through  $w(\mathcal{S}) = \tilde{R}^{-1}w^*(\mathcal{S})$ . Using two times the Jacobian chain rule,

$$\nabla_{W_\sigma(\mathcal{S})} l(z|w(\mathcal{S}), \beta, \tau) = J_{W_\sigma(\mathcal{S})}^T \sigma^2(\mathcal{S}) J_{\sigma^2(\mathcal{S})}^T w(\mathcal{S}) \nabla_{w(\mathcal{S})} l(z|w(\mathcal{S}), \beta, \tau).$$

From  $\log(\sigma^2(s)) = W_\sigma(s) + X_\sigma(s)\beta_\sigma^T$ , we have

$$J_{W_\sigma(\mathcal{S})}^T \sigma^2(\mathcal{S}) = \text{diag}(\sigma^2(\mathcal{S})).$$

From the use of the ancillary parametrization, we have

$$J_{\sigma^2(\mathcal{S})}^T w(\mathcal{S}) = J_{\sigma^2(\mathcal{S})}^T (\tilde{R}_0^{-1}w^*) \circ \sigma(\mathcal{S}) = \text{diag}((\tilde{R}_0^{-1}w^*) \circ \sigma^{-1}(\mathcal{S})/2).$$

Combining the two previous expressions, we have

$$J_{W_\sigma(\mathcal{S})}^T \sigma^2(\mathcal{S}) J_{\sigma^2(\mathcal{S})}^T w(\mathcal{S}) = \text{diag}((\tilde{R}_0^{-1}w^*) \circ \sigma(\mathcal{S})/2) = \text{diag}(w/2),$$

eventually leading to the result.

### S4.3 Gradient of the negated log-density with respect to $\log(\alpha)$

*Sufficient augmentation.* In sufficient augmentation, the range intervenes in the NNGP prior of the latent field. The gradient is:

$$-\frac{\partial g_\alpha^{\text{sufficient}}(\log(\alpha))}{\partial \log(\alpha)(s_i)} = \left( w^T \tilde{R}^T \right) \left( \partial \tilde{R} / \partial \log(\alpha)(s_i) \right) w + \sum_{j/s_j \in \{s_i \cup \text{ch}(s_i)\}} \left( \partial \tilde{R}_{j,j} / \partial \log(\alpha)(s_i) \right) / \tilde{R}_{j,j}. \quad (\text{S6})$$

Start from the negated log density of the latent field with sufficient augmentation:

$$-g_{\alpha}^{\text{sufficient}}(\log(\alpha)(\mathcal{S})) = \log\left(|\tilde{R}(\mathcal{S}, \alpha(\mathcal{S}))|\right) + w^T \tilde{R}(\mathcal{S}, \alpha(\mathcal{S}))^T \tilde{R}(\mathcal{S}, \alpha(\mathcal{S})) w \times 1/2.$$

Let us write the derivative of the log-determinant  $\log(|\tilde{R}|)$ :

$$\begin{aligned} \partial \log(|\tilde{R}|) / \partial \log(\alpha(s_j)) &= \partial(\sum_{i=1}^n \log(\tilde{R}_{i,i})) / \partial \log(\alpha(s_j)) \text{ (because } \tilde{R} \text{ is triangular)} \\ &= \sum_{i=1}^n \partial \log(\tilde{R}_{i,i}) / \partial \log(\alpha(s_j)) \\ &\quad \text{(only the rows corresponding to } s_j \text{ and its children are affected)} \\ &= \sum_{i/s_i \in \{s_j \cup \text{ch}(s_j)\}} \partial \log(\tilde{R}_{i,i}) / \partial \log(\alpha(s_j)) \\ &\quad \text{log-function derivative} \\ &= \sum_{i/s_i \in \{s_j \cup \text{ch}(s_j)\}} \left( \partial \tilde{R}_{i,i} / \partial \log(\alpha(s_j)) \right) / \tilde{R}_{i,i} \end{aligned}$$

Let us write the derivative of  $w^T \tilde{R}^T \tilde{R} w \times 1/2$ :

$$\begin{aligned} \partial \left( w^T \tilde{R}^T \tilde{R} w \times 1/2 \right) / \partial \log(\alpha(s_j)) &= \partial \left( (w^T \tilde{R}^T) (\tilde{R} w) \times 1/2 \right) \partial \log(\alpha(s_j)) \\ &= \partial(w^T \tilde{R}^T) / \partial \log(\alpha(s_j)) (\tilde{R} w) \times 1/2 + \\ &\quad (w^T \tilde{R}^T) \partial(\tilde{R} w) / \partial \log(\alpha(s_j)) \times 1/2 \\ &= (w^T \tilde{R}^T) \partial(\tilde{R} w) / \partial \log(\alpha(s_j)) \\ &= (w^T \tilde{R}^T) (\partial \tilde{R} / \partial \log(\alpha(s_j)) w) \end{aligned}$$

*Ancillary Augmentation.* When ancillary augmentation is used, the covariance parameters intervene in the density of the observations knowing the latent field. This induces:

$$-\partial h_{\alpha}^{\text{ancillary}}(\log(\alpha)) / \partial \log(\alpha)(s_i) = \nabla_w l(z(s_i) | w, \beta, \tau)^T \tilde{R}^{-1} \left( \partial \tilde{R} / \partial \log(\alpha)(s_i) \right) w, \quad (\text{S7})$$

Start from

$$-h_{\alpha}^{\text{ancillary}}(\log(\alpha)) = -l(z | w = \tilde{R}^{-1} w^*, X, \beta, \tau).$$

Applying differentiation, we get

$$\begin{aligned}
& \partial \left( -l(z|w = \tilde{R}^{-1}w^*, X, \beta, \tau) \right) / \partial(\log(\alpha(s_j))) \\
& \text{(Conditional independence)} \\
& = \sum_{i=1}^n \sum_{x \in \text{obs}(s_i)} - \partial \left( l(z_x|w(s_i) = \left( \tilde{R}^{-1}w^* \right)_i, X, \beta, \tau) \right) / \partial(\log(\alpha(s_j))) \\
& \text{(Chain rule)} \\
& = \sum_{i=1}^n - \partial \left( \tilde{R}^{-1}w^* \right)_i / \partial(\log(\alpha(s_j))) \times \\
& \quad \sum_{x \in \text{obs}(s_i)} \partial \left( l(z_x|w(s_i) = \left( \tilde{R}^{-1}w^* \right)_i, X, \beta, \tau) \right) / \partial(w(s_i)) \\
& \text{($w^*$ is not changed by $\theta$)} \\
& = \sum_{i=1}^n - \left( \partial \tilde{R}^{-1} / \partial(\log(\alpha(s_j))) w^* \right)_i \times \\
& \quad \sum_{x \in \text{obs}(s_i)} \partial \left( l(z_x|w(s_i) = \left( \tilde{R}^{-1}w^* \right)_i, X, \beta, \tau) \right) / \partial(w(s_i)) \\
& \text{(Differentiation of inverse)} \\
& = \sum_{i=1}^n \left( \tilde{R}^{-1} \partial \tilde{R} / \partial(\log(\alpha(s_j))) \tilde{R}^{-1} w^* \right)_i \times \\
& \quad \sum_{x \in \text{obs}(s_i)} \partial \left( l(z_x|w(s_i) = \left( \tilde{R}^{-1}w^* \right)_i, X, \beta, \tau) \right) / \partial(w(s_i)) \\
& \text{(Recognising gradient of $l(\cdot)$ in $w$)} \\
& = \nabla_w l(z|\tilde{R}^{-1}w^*, X, \beta, \tau) \tilde{R}^{-1} \partial \tilde{R} / \partial(\log(\alpha(s_j))) \tilde{R}^{-1} w^*.
\end{aligned}$$

#### S4.4 Computational cost of the gradient of the negated log-density with respect to $\log(\alpha)$

Both sufficient and ancillary formulations have a partial derivative with a term under the shape:

$$u^T \partial \tilde{R} / \partial(\log(\alpha(s_j))) v,$$

with  $u$  an  $v$  two vectors with affordable cost.

Due to its construction,  $\partial \tilde{R} / \partial(\log(\alpha(s_j)))$  has non-null rows only at the rows that correspond to  $s_j$  and  $ch(s_j)$ , and each of those rows has itself at most  $m + 1$  non-null coefficients. Sparse matrix-vector multiplication  $(\partial \tilde{R} / \partial(\log(\alpha(s_j))))v$  therefore costs  $O((m + 1) \times (1 + |ch(s_j)|))$  operations. Given the fact that  $\sum_{j=1}^n |ch(s_j)| = \sum_{j=1}^n |pa(s_j)| = n \times m$ , we can expect

that the computational cost needed to compute  $(\partial\tilde{R}/\partial(\log(\alpha(s_j))))v$  for  $j \in 1, \dots, n$  will be  $O(n \times (m + 1)^2)$  operations, which is affordable.

Moreover, due to the fact that  $\partial\tilde{R}/\partial(\log(\alpha(s_j)))$  has non-null rows only at the rows that correspond to  $s_j$  and  $ch(s_j)$ , we can deduce that  $(\partial\tilde{R}/\partial(\log(\alpha(s_j))))v$  has non-null terms only on the slots that correspond to  $s_i$  and its children. Computing  $u^T(\partial\tilde{R}/\partial(\log(\alpha(s_j))))v$  will then cost  $O(ch(s_j) + 1)$  operations. Using again  $\sum_{j=1}^n |ch(s_j)| = \sum_{j=1}^n |pa(s_j)| = n \times m$ , we can deduce that (if we know already  $(\partial\tilde{R}/\partial(\log(\alpha(s_j))))v$ ) computing  $u^T(\partial\tilde{R}/\partial(\log(\alpha(s_j))))v$  for  $j \in 1, \dots, n$  will cost  $O(n(m + 1))$ .

## S4.5 General derivative of $\tilde{R}$ with respect to nonstationary range parameters

The aim is to find  $\partial\tilde{R}/\partial\log(\alpha(s_j))$  with  $j \in 1, \dots, n$ . Let us focus on the  $i^{th}$  row of  $\tilde{R}$ , noted  $\tilde{R}_{i,\cdot}$ . The index of the row  $i$  can be different from  $j$ . To find the derivative of  $\tilde{R}_{i,\cdot}$  with respect to  $\log(\alpha(s_j))$ , we need to use the covariance matrix between  $s_i$  and its parents  $pa(s_i)$ .

Let us note  $\Sigma^i$  the covariance matrix corresponding to  $(pa(s_i), s_i)$ , and Let us block it as

$$\Sigma^i = \left[ \begin{array}{c|c} \Sigma_{11}^i & \Sigma_{12}^i \\ \hline \Sigma_{21}^i & \Sigma_{22}^i \end{array} \right] \quad \Sigma_{11}^i \text{ being a } m \times m, \text{ with } m = |pa(s_i)|, \text{ covariance matrix corresponding}$$

to  $pa(s_i)$ , and  $\Sigma_{22}^i$  being a  $1 \times 1$  matrix corresponding to  $s_i$ . From its construction,  $\tilde{R}_{i,\cdot}$

has non-null coefficients only for the column entries that correspond to  $s_i$  and its parents  $pa(s_i)$ . Therefore there is no need to compute the gradient but for those coefficients. The

diagonal element  $\tilde{R}_{i,i}$  has value  $1/\bar{\sigma}_i$ ,  $\bar{\sigma}_i$  being the standard deviation of  $w(s_i)$  conditionally on  $w(pa(s_i))$ . The elements that correspond to  $pa(s_i)$  have value  $-\Sigma_{21}^i(\Sigma_{11}^i)^{-1}/\bar{\sigma}_i$ .

Let us start with the diagonal coefficient  $\tilde{R}_{i,i}$ :

$$\begin{aligned}
\partial(\tilde{R}_{ii})/\partial\log(\alpha(s_j)) &= \partial((\bar{\sigma}_i^2)^{-1/2})/\partial\log(\alpha(s_j)) \\
&\quad \text{(chain rule)} \\
&= -(\bar{\sigma}_i^{-3}/2) \times \partial(\bar{\sigma}_i^2)/\partial\log(\alpha(s_j)) \\
&\quad \text{(using conditional variance formula)} \\
&= -(\bar{\sigma}_i^{-3}/2) \times \partial(\Sigma_{22}^i - \Sigma_{21}^i(\Sigma_{11}^i)^{-1}\Sigma_{12}^i)/\partial\log(\alpha(s_j)) \\
&\quad \text{(product rule)} \\
&= -(\bar{\sigma}_i^{-3}/2) \times \partial(\Sigma_{22}^i)/\partial\log(\alpha(s_j)) \\
&\quad + (\bar{\sigma}_i^{-3}) \times \partial(\Sigma_{21}^i)/\partial\log(\alpha(s_j))(\Sigma_{11}^i)^{-1}\Sigma_{12}^i \\
&\quad + (\bar{\sigma}_i^{-3}/2) \times \Sigma_{21}^i \partial((\Sigma_{11}^i)^{-1})/\partial\log(\alpha(s_j))\Sigma_{12}^i \\
&\quad \text{(derivative of inverse)} \\
&= -(\bar{\sigma}_i^{-3}/2) \times \partial(\Sigma_{22}^i)/\partial\log(\alpha(s_j)) \tag{a} \\
&\quad + (\bar{\sigma}_i^{-3}) \times \partial(\Sigma_{21}^i)/\partial\log(\alpha(s_j))(\Sigma_{11}^i)^{-1}\Sigma_{12}^i \tag{b} \\
&\quad - (\bar{\sigma}_i^{-3}/2) \times \Sigma_{21}^i(\Sigma_{11}^i)^{-1} (\partial(\Sigma_{11}^i)/\partial\log(\alpha(s_j))) (\Sigma_{11}^i)^{-1}\Sigma_{12}^i \tag{c}
\end{aligned}$$

Let us now differentiate the coefficients that correspond to  $pa(s_i)$ , located on row  $\tilde{R}_{i\cdot}$  at the left of the diagonal:

$$\begin{aligned}
\partial(-\Sigma_{21}^i(\Sigma_{11}^i)^{-1}/\bar{\sigma}_i)/\partial\log(\alpha(s_j)) &= -\partial(\Sigma_{21}^i(\Sigma_{11}^i)^{-1} \times \tilde{R}_{ii})/\partial\log(\alpha(s_j)) \\
&\quad \text{(product rule)} \\
&= -(\partial\Sigma_{21}^i/\partial\log(\alpha(s_j))) (\Sigma_{11}^i)^{-1} \times \tilde{R}_{ii} \\
&\quad - \Sigma_{21}^i (\partial((\Sigma_{11}^i)^{-1})/\partial\log(\alpha(s_j))) \times \tilde{R}_{ii} \\
&\quad - \Sigma_{21}^i(\Sigma_{11}^i)^{-1} \partial\tilde{R}_{ii}/\partial\log(\alpha(s_j)) \\
&\quad \text{(derivative of inverse)} \\
&= -(\partial\Sigma_{21}^i/\partial\log(\alpha(s_j))) (\Sigma_{11}^i)^{-1} \times \tilde{R}_{ii} \tag{d} \\
&\quad + \Sigma_{21}^i(\Sigma_{11}^i)^{-1} (\partial\Sigma_{11}^i/\partial\log(\alpha(s_j))) (\Sigma_{11}^i)^{-1} \times \tilde{R}_{ii} \tag{e} \\
&\quad - \Sigma_{21}^i(\Sigma_{11}^i)^{-1} \times \underbrace{\partial\tilde{R}_{ii}/\partial\log(\alpha(s_j))}_{\text{already known}} \tag{f}
\end{aligned}$$

From those derivatives, it appears that the elements that are needed to get the derivative

of  $\tilde{R}_{i\cdot}$ , are  $(\Sigma^i)^{-1}$  and  $\partial\Sigma^i/\partial\log(\alpha(s_j))$  (with  $s_j \in s_i \cup pa(s_i)$ ). The former can anyway be re-used in order to obtain  $\tilde{R}$ . The latter can be approximated using finite differences:

$$\partial\Sigma^i/\partial\log(\alpha(s_j)) \approx (\Sigma^i(\log(\alpha(s_j)) + d\log(\alpha(s_j))) - \Sigma^i(\log(\alpha(s_j)))) / d\log(\alpha(s_j)).$$

## S4.6 Computational cost of the derivative of $\tilde{R}$ with respect to nonstationary range parameters

We can see that the differentiation of  $\tilde{R}_{i\cdot}$  is non-null only for  $\alpha(pa(s_i) \cup s_i)$  because the entries of  $\Sigma^i$  are given by  $K(s, t, \alpha(s), \alpha(t))$  with  $s, t \in s_i \cup pa(s_i)$ . Conversely, if  $\log(\alpha(s_j))$  moves, only the rows of  $\tilde{R}$  that correspond to  $s_i$  and its children on the DAG move as well. This means that in order to compute the derivative of  $\tilde{R}$  with respect to  $\alpha_j$ , the row differentiation operation must be done  $|ch(s_j)| + 1$  times and not  $n$  times. Knowing the fact that  $\sum_{j=1}^n |ch(s_j)| = \sum_{j=1}^n |pa(s_j)| = m \times n$  ( $m$  being the number of nearest neighbours used in Vecchia approximation), we can see that row differentiation must be done  $(m + 1) \times n$  times in order to get all the derivatives of  $\tilde{R}$  with respect to  $\alpha(s_1, \dots, s_n)$ . Given the fact that one row has  $m + 1$  non-null terms and that  $(m + 1) \times n$  rows are differentiated, the cost in RAM to store the differentiation of  $\tilde{R}$  will be  $O(m + 1)^2 n$ . On the other hand, the flop cost of differentiation itself may seem daunting. However, the fact that spatially-variable covariance parameters affect pairwise covariances considerably simplifies the problem. In the derivatives, there are only 3 terms that depend on  $\alpha(s_j)$ , they are  $\partial(\Sigma_{22}^i)/\partial\log(\alpha(s_j))$ ,  $\partial(\Sigma_{12}^i)/\partial\log(\alpha(s_j))$ , and  $\partial(\Sigma_{11}^i)/\partial\log(\alpha(s_j))$ . Let us separate the cases:

1. When  $i \neq j$

(a)  $\partial(\Sigma_{12}^i)/\partial\log(\alpha(s_j))$  has only one non-null coefficient.

(b)  $\partial(\Sigma_{11}^i)/\partial\log(\alpha(s_j))$  is a  $m \times m$  matrix with cross structure (non-null coefficients only for the row and the column corresponding to  $s_j$ ).

(c)  $\partial(\Sigma_{22}^i)/\partial\log(\alpha(s_j))$  is a null  $1 \times 1$  matrix.

2. When  $i = j$

(a)  $\partial(\Sigma_{12}^i)/\partial\log(\alpha(s_j))$  is a dense vector of length  $m$ .

(b)  $\partial(\Sigma_{11}^i)/\partial\log(\alpha(s_j))$  is null.

(c)  $\partial(\Sigma_{22}^i)/\partial\log(\alpha(s_j))$  is null. Because a change in  $\log(\alpha)(s_i)$  does not affect the marginal variance of  $w(s_i)$  (a change in  $w_{\sigma^2(s_i)}$  does).

The costliest part of the formulas is to compute  $(\Sigma_{11}^i)^{-1}$ . However, this part needs only to be computed one time since it is not affected by differentiation. Even better,  $(\Sigma_{11}^i)^{-1}$  and  $\Sigma_{21}^i(\Sigma_{11}^i)^{-1}$  can be used to compute  $\tilde{R}$  and then recycled on the fly to compute the derivatives. The computational effort needed to get them can then be removed from the cost of the derivative and remain in the cost of  $\tilde{R}$ .

Applying all those remarks gives table S3.

Table S3: costs to compute  $\partial\tilde{R}_{i.}/\partial(\log(\alpha(s_j)))$

	(a)	(b)	(c)	(d)	(e)	(f)
$i = j$	$O(1)$	$O(m)$	0	$O(m^2)$	0	0
$s_i \in ch(s_j)$	0	$O(1)$	$O(m)$	$O(m)$	$O(m)$	0

Using table S3 and again  $\sum_{j=1}^n |ch(s_j)| = \sum_{j=1}^n |pa(s_j)| = m \times n$ , we can see that the matrix operations should have a total cost of  $O(m^2 \times n)$ . The cost of the finite difference approximation to  $\partial\Sigma^i/\partial\log(\alpha(s_j))$  must be added to this. The cost of computing the finite differences in one coefficient of  $\Sigma^i$  depends on whether isotropic or anisotropic range parameters are used. In the case of isotropic range parameters, only a recomputation of the covariance function (6) with range  $\exp(\log(\alpha(s) + dw))$  instead of  $\exp(\log(\alpha(s)))$  will be needed. In the other case, the SVD of  $\log(A)$  must be computed again. What's more, the covariance function (5) involves the Mahalanobis distance instead of the Euclidean distance. The cost

will then depend on  $d$ , and be higher than in the case with isotropic covariance parameters. However, due to (4), it appears that if  $\log(\alpha)(s_j)$  moves, only the row and column of  $\Sigma^i$  that correspond to  $s_j$  will be affected. Moreover, due to the symmetry of  $\Sigma^i$ , the row and the column will be changed exactly the same way. Therefore, computing  $\partial\Sigma^i/\partial\log(\alpha(s_j))$  involves only  $m + 1$  finite differences since  $\Sigma^i$  is of size  $(m + 1) \times (m + 1)$ .

The finite difference  $\partial\Sigma^i/\partial\log(\alpha(s_j))$  must be computed  $m + 1$  time for each row of  $\tilde{R}$ , and there is  $n$  rows. Therefore, the total cost of the finite differences should be  $O(m + 1)^2n$

Therefore, we can hope that careful implementation of the derivative of  $\partial\tilde{R}/\partial(\alpha(s_1, \dots, s_n))$  will cost  $O(n(m + 1)^2)$  operations, in the same order as computing  $\tilde{R}$  itself (Guinness, 2018).

## S4.7 Gradient of the negated log-density with respect to $\log(\tau^2)$

Here, only the sufficient parametrization is used. Due to the fact that there can be more than one observation per spatial site, we consider an index  $x$  ranging between 1 and the number of observations, and the spatial site  $s$  such that the observation  $x$  is done at the site  $s$ .

$$-\partial h^{sufficient}(\log(\tau^2))/\partial\log(\tau^2(x)) = 1/2 - (z(x) - w(s) - X(x)\beta)^2/2\tau^2(x). \quad (\text{S8})$$

We start from the log-density of the observed field knowing its mean and its variance as described in (11):

$$h^{sufficient}(\log(\tau^2)) = l(z|w(\mathcal{S}), \beta, \tau).$$

Using the conditional independence of  $z$  knowing the parameters of the model, we have

$$\partial l(z|w(\mathcal{S}), \beta, \tau^2)/\partial\log(\tau^2(x)) = \partial l(z(x)|w(s), \beta, \tau^2(x))/\partial\log(\tau^2(x)).$$

Introducing the Gaussian formula for  $l(\cdot)$ , we get

$$\partial l(z(x)|w(s), \beta, \tau^2(x))/\partial \log(\tau^2(x)) = \partial \frac{(z(x) - X(x)\beta - w)^2}{2\tau^2(x)} - \frac{\log(\tau^2(x))}{2} / \partial \log(\tau^2(x)).$$

## S5 EXPERIMENTS ON SYNTHETIC DATA SETS

### S5.1 Objectives

We would like to investigate the improvements caused by using nonstationary modeling when it is relevant, the problems caused by using nonstationary modeling when it is irrelevant, and the potential identification and overfitting problems of the model we devised. Our general approach to find answers to those questions is to run our implementation on synthetic data sets and analyze their results. Following the nonstationary process and data model we defined using (11) and (12), there is 12 possible configurations counting the full stationary case: 2 marginal variance models, 2 noise variance models, 3 range models. In order to keep the Section readable, we use the following notation for the different models:

- $(\emptyset)$  is the stationary model.
- $(\sigma^2)$  is a model with nonstationary marginal variance.
- $(\tau^2)$  is a model with heteroskedastic noise variance.
- $(\alpha)$  is a model with nonstationary range and isotropic range parameters.
- $(A)$  is a model with nonstationary range and elliptic range parameters.
- Complex models are noted using “+”. For example, a model with nonstationary marginal variance and heteroskedastic noise variance is noted  $(\sigma^2 + \tau^2)$ .

## S5.2 Method

Our approach here is to use a possibly misspecified model and see what happens. Four cases are possible:

- The “right” model, in the sense it matches perfectly the process used to generate the data (however, potential identification and overfitting problems may cause it to be a bad model in practice).
- “Wrong” models, where some parameters that are stationary in the data are non-stationary in the model, and some parameters that are stationary in the model are non-stationary in the data.
- Under-modeling, where some parameters that are stationary in the model are non-stationary in the data, but all parameters that are stationary in the data are stationary in the model.
- Over-modeling, where some parameters that are stationary in the data are non-stationary in the model, but all parameters that are stationary in the model are stationary in the data.

If a nonstationary model is needed for data analysis, we should see if the “right” model does better than “under-modeling”. The problem of overfitting will be assessed by comparing over-modeling, under-modeling, and the “right” model. If there is some overfitting, over-modeling or even “right” modeling would have worse performances than simpler models. Identification problems will be monitored by looking at the “wrong” models and under-modeling. If some model formulations are interchangeable, then some of the “wrong” models should perform as good as the “right” model. Also, if two parametrizations are equivalent, then using either parametrization should do as good as using both, therefore under-modeling should do as good as the “true” model.

The models are compared using several indicators. The first is the Deviance Information Criterion (DIC) (Spiegelhalter et al., 1998). The latent field retrieval is assessed using the smoothing MSE and the prediction MSE. The covariance parameter retrieval is assessed by treating these parameters as latent fields and using smoothing MSE, no prediction was done because of the very high spatial coherence of those latent fields. Eventually, credible interval coverage is studied for the high-level parameters, that is the response, range, noise, and latent field variance intercept, and the covariance parameters variance. The MSEs are derived as follows. The observations of the model at the observed sites  $\mathcal{S}$  are disrupted by the white noise  $\epsilon$ . The true latent field, used to generate the data, is named  $w_{true}$ . The estimated latent field is named  $\hat{w}$ . The smoothing MSE is

$$MSE_{smooth} = \frac{1}{\#\mathcal{S}} \sum_{s \in \mathcal{S}} (\hat{w}(s) - w_{true}(s))^2.$$

The smoothing MSE is also used to assess the estimation of the spatially-indexed covariance parameters  $\theta$

$$MSE_{\theta} = \frac{1}{\#\mathcal{S}} \sum_{s \in \mathcal{S}} (\log(\hat{\theta}(s)) - \log(\theta_{true}(s)))^2,$$

and log noise variance  $\tau^2$

$$MSE_{\tau} = \frac{1}{\#\mathcal{S}} \sum_{s \in \mathcal{S}} (\log(\hat{\tau}^2(s)) - \log(\tau_{true}^2(s)))^2.$$

The field is also predicted at unobserved sites  $\mathcal{P}$ , giving the prediction MSE

$$MSE_{pred} = \frac{1}{\#\mathcal{P}} \sum_{s \in \mathcal{P}} (\hat{w}(s) - w_{true}(s))^2.$$

The results are analyzed using simple linear models. In an experiment, for each type of data, each measure of performance is regressed on the seed and the model formulation. The seed is an useful control variable, some data sets being "trickier" than others. We do

not report the associated coefficients. In each case, we choose the “right” model to be the reference factor. The p-values are reported. For example, in the first experiment, there are eight types of data  $((\emptyset), (\sigma^2), (\tau^2), (\alpha), (\sigma^2 + \tau^2), (\tau^2 + \alpha), (\sigma^2 + \alpha)$  and  $(\sigma^2 + \tau^2 + \alpha))$  and six measures of the performance (the DIC, the smoothing MSE, the prediction MSE, the noise, range, and scale MSE). Therefore, forty-eight linear models are run. That is, in table S4, each column of the sub-tables correspond to the coefficients of a linear model.

The following method was used to create one synthetic data set.

1. 12000 locations are drawn uniformly on a square whose sides have length 5.
2. The 10000 first locations are kept for training. 20000 observations are done at these locations. First, each location is granted an observation. Then, each of the 10000 remaining observations is assigned to a location chosen following an uniform multinomial distribution.
3. Predictive Process bases  $B$  for the parameter latent fields are defined. The marginal variance is unitary, the range is equal to 0.5, and the Matérn smoothness is equal to 1.5. There are 49 knots.
4. The parameter fields are sampled:
  - The spatial range  $\log(\alpha) = \log(.1) + \sqrt{\gamma_\alpha} BW_\alpha^*$ , with  $W_\alpha^* \stackrel{ind}{\sim} \mathcal{N}(0, 1)$
  - The process marginal variance  $\log(\sigma) = \log(10) + \sqrt{\gamma_\sigma} BW_\sigma^*$ , with  $W_\sigma^* \stackrel{ind}{\sim} \mathcal{N}(0, 1)$
  - The noise variance  $\log(\tau) = \log(10) + \sqrt{\gamma_\tau} BW_\tau^*$ , with  $W_\tau^* \stackrel{ind}{\sim} \mathcal{N}(0, 1)$

If  $\gamma = 0$  then the parameter field is stationary.

5. The nonstationary NNGP latent field  $w_{true}$  is sampled using  $\alpha$  and  $\sigma$ , using a Matern function with smoothness 1.5 as the isotropic kernel of (5).
6. The response variable is sampled by adding a Gaussian noise with variance  $diag(\tau^2)$  to the latent field.

We started with the eight models obtained by combining  $(\sigma)$ ,  $(\alpha)$ , and  $(\tau)$ , giving us  $(\emptyset)$ ,  $(\sigma^2)$ ,  $(\tau^2)$ ,  $(\alpha)$ ,  $(\sigma^2 + \tau^2)$ ,  $(\tau^2 + \alpha)$ ,  $(\sigma^2 + \alpha)$ , and  $(\sigma^2 + \tau^2 + \alpha)$ . We tested each data-model configuration, yielding 64 situations in total. 49 spatial basis functions were used to sample the latent parameter fields. Each case was replicated 60 times. Second, we focused on the case of elliptic range parameters with the three models obtained by combining  $(\alpha)$  and  $(A)$ , giving us  $(\emptyset)$ ,  $(\alpha)$ , and  $(A)$ . Like before, we tested the 9 data-model configurations 60 times each.

### S5.3 Results

The results are presented in tables S4, S5, S6, and S7.

Table S4 presents results for settings combining nonstationary, locally isotropic correlation, nonstationary variance of the latent field, and heteroskedasticity of the noise. We can see that in general under-modeling (in gray) or “wrong” modeling (in brown) impairs the model performance in terms of smoothing MSE (table S4a), prediction MSE (table S4b), and DIC (Table S4c), usually with good significance. We also can see that over-modeling, in blue has little effect on performance. The same conclusions also seem to hold for the estimation of the fields of covariance parameters (tables S4d, S4e, S4f), which is less surprising.

The 95% *a posteriori* coverage of the high-level parameters are presented in the isotropic runs S5. An important feature is that picking the “right model” (in green) or over-modeling (in blue) seem to provide satisfying coverage. Under-modeling or picking a “wrong” model, on the other hand, deteriorate the coverage. An important point to take into account is that in tables S5d, S5e, and S5f, some of the zeroes and ones are due to model formulation, while others are due to genuine model performance. In table S5f, the bottom-right corner is filled with ones, because the data sets are generated without nonstationarity in the noise, and the model being stationary can only correctly estimate the variance of the noise PP. On the other hand, the top-right corner is filled with zeroes, because the models are nonstationary

and even if their estimate of the variance is extremely low, it will never include the null variance in their *a posteriori* intervals. The bottom-left corner is filled with zeroes because a stationary model cannot retrieve a non-null variance for the noise variance PP. Eventually, the ones on the top-left quadrant are informative, and tell, along with other high coefficients, that there is some over-coverage.

The analysis of the performance of the anisotropic runs, in table S6, shows modest yet significant improvements of the model to predict the latent field in relevant cases. The DIC is also improved. On the other hand, over-modelling does not increase the error criteria, or very slightly and with little significance in general. This is due to the ability of the model to regress towards a stationary state. Eventually, the parameter MSE show interesting results in term of parameter estimation. Table S6d shows that the locally anisotropic model is able to capture, to some extent, the parameters driving the anisotropy. What is more surprising is that S6c shows that it also improves the retrieval of the ellipse diameter, with respect to the locally isotropic model especially. Like before, over-modeling causes no problem. As a conclusion, using the locally anisotropic model will -slightly- improve prediction, but greatly boost the estimation of the covariance structure.

The coverage results of the anisotropic runs, presented in table S7, need some clarification. The 6 range variance parameters correspond to the half-vectorization of the range variance. In the stationary case, the range matrix is a  $3 \times 3$  null matrix. In the locally isotropic case, only its upper-left corner is non-null. In the anisotropic case, its diagonal is non-null. The ones in the six tables ranging from S7d to S7i are “false” due to model formulation. It is worth noticing that the upper-left coefficients of tables S7g and S7i are below the target 0.95. Those parameters control the intensity of the anisotropy in the range latent field. This is quite coherent with the trace plots such as figure 3(c): there, the true log-variance is 0, and we can see that the two PP variance parameters associated with anisotropy are mixing between  $-2$  and 0. Other runs confirmed this behavior. The three range intercepts, from table S7a

to S7c, correspond to the three components of the range parameter. The first component retrieves the ellipse determinant, while the other two parametrize the anisotropy. The ones are, once again, “false”. The notable point is that, in table S7a, we can see that using the right model formulation considerably improves the coverage of the determinant of the range ellipse. The same remark goes for the latent field’s variance intercept (figure S7j) and noise variance intercept (figure S7k). Overall, even if the elliptic model tends to undershoot its anisotropy variance parameters, it improves the coverage of the other parameters.

## S5.4 Identification between range and variance

Even though it seems difficult to identify nonstationary range and variance, a troubling observation shows that there is some kind of identification: when given the possibility, the model is able to make the right choice between the two parameters. In Figure S1, we used boxplots to summarize results of the models that estimate both nonstationary marginal variance and range. On the left (Figure S1(a)), we can see estimates for the log-variance of  $W_\alpha$ ’s log-GP prior. On the right (Figure S1(b)), we see its counterpart for  $W_\sigma$ . In both subfigures, the boxplots are separated following the type of the data, ( $\emptyset$ ) being stationary data, ( $\alpha$ ) being data with nonstationary range, ( $\sigma^2$ ) being data with nonstationary variance, and ( $\alpha + \sigma^2$ ) being data with both nonstationarities. Recall that when the log-variance is low, the corresponding field is practically stationary. Then we can see that the right kind of nonstationarity is detected for all four configurations: when data is stationary, both log variances are very low, when the data is ( $\sigma^2$ ), then only the log-variance of  $W_\sigma$  is high, etc.

## S6 Construction of a Predictive Process basis

We pursue a truncated Predictive Process (PP) basis (Banerjee et al., 2008), itself obtained from a NNGP. While the PP approximations are prone to over-smoothing (see the discussions in Datta et al., 2016; ?), this is not a problem here since the hyperprior range and smoothness

		Type of data							
		$\alpha + \sigma + \tau$	$\sigma + \tau$	$\alpha + \tau$	$\tau$	$\alpha + \sigma$	$\sigma$	$\alpha$	$\emptyset$
Type of model	$\alpha + \sigma + \tau$	0	0	0	0.01	0	0	0	0
	$\sigma + \tau$	0.01	0	0.02	0.01	0.02*	0	0.02**	0
	$\alpha + \tau$	0.02	0.09**	0	0.01	0.01	0.08***	0	0
	$\tau$	0.13**	0.05*	0.02	0	0.13***	0.06**	0.03**	0
	$\alpha + \sigma$	0.13**	0.14***	0.15***	0.14***	0	0	0	0
	$\sigma$	0.14**	0.1**	0.11**	0.14***	0.02	0	0.03**	0
	$\alpha$	0.12**	0.2***	0.14***	0.18***	0.01	0.07***	0	0
	$\emptyset$	0.13**	0.07**	0.06**	0.04	0.08***	0.03**	0.03**	0

a Latent field smoothing.

		Type of data							
		$\alpha + \sigma + \tau$	$\sigma + \tau$	$\alpha + \tau$	$\tau$	$\alpha + \sigma$	$\sigma$	$\alpha$	$\emptyset$
Type of model	$\alpha + \sigma + \tau$	0	-0.01	0.01	0.01	-0.06	0.01	0.01	0
	$\sigma + \tau$	0.05	0	0.04	0.01	0.08	-0.01	0.02	0
	$\alpha + \tau$	0.03	0.08*	0	0.01	-0.1	0.06	0	0
	$\tau$	0.02	0.01	0.01	0	-0.03	0.06	0.04	0
	$\alpha + \sigma$	0.04	0.04	0.06**	0.06***	0	-0.02	0	0
	$\sigma$	0.09	0.04	0.08**	0.07***	0	0	0.04*	0
	$\alpha$	0.05	0.13**	0.06**	0.08***	-0.05	0.09*	0	0
	$\emptyset$	0.18**	0.04	0.04	0.02**	0.05	0.02	0.02	0

b Latent field prediction.

		Type of data							
		$\alpha + \sigma + \tau$	$\sigma + \tau$	$\alpha + \tau$	$\tau$	$\alpha + \sigma$	$\sigma$	$\alpha$	$\emptyset$
Type of model	$\alpha + \sigma + \tau$	0	-606	186	2634	-165	18	18	-12
	$\sigma + \tau$	-1916	0	-1090	2038	103	5	114	3
	$\alpha + \tau$	-666	1245	0	2398	-59	43	-5	-11
	$\tau$	70	159	-252	0	1370***	961***	443**	-31
	$\alpha + \sigma$	3887**	5861**	5362**	6081**	0	23	18	10
	$\sigma$	4994**	5142**	4238**	8155**	15	0	242*	22
	$\alpha$	3361*	6344**	4417**	7264**	-3	211*	0	-9
	$\emptyset$	6684**	7183**	6532**	8250**	1185***	658**	472**	0

c DIC.

		Type of data							
		$\alpha + \sigma + \tau$	$\sigma + \tau$	$\alpha + \tau$	$\tau$	$\alpha + \sigma$	$\sigma$	$\alpha$	$\emptyset$
Type of model	$\alpha + \sigma + \tau$	0	0	0.01	0.01	0.02	0	0	0
	$\sigma + \tau$	0.72 **	0	0.8 **	0	0.74 **	0	0.83 ***	0
	$\alpha + \tau$	3.15 ***	2.62 ***	0	0	2.38 ***	2.92 ***	0	0
	$\tau$	0.78 **	0.01	0.82 **	0	0.78 **	0	0.84 ***	0
	$\alpha + \sigma$	0.68 **	0.65 **	0.78 **	0.59 **	0	0	0	0
	$\sigma$	0.74 **	0.01	0.81 **	0.02	0.77 **	0	0.83 ***	0
	$\alpha$	4.49 ***	3.8 ***	2.04 ***	2.04 ***	2.86 ***	3.36 ***	0	0
	$\emptyset$	0.77 **	-0.01	0.79 **	0	0.77 **	0	0.78 ***	0

d Log-range smoothing MSE.

		Type of data							
		$\alpha + \sigma + \tau$	$\sigma + \tau$	$\alpha + \tau$	$\tau$	$\alpha + \sigma$	$\sigma$	$\alpha$	$\emptyset$
Type of model	$\alpha + \sigma + \tau$	0	0	0.01	0	0	0	0	0 **
	$\sigma + \tau$	0.17	0	0.19 **	0	0.18	0	0.21 ***	0 **
	$\alpha + \tau$	1.95 ***	1.79 ***	0	0	1.48 ***	2.03 ***	0	0
	$\tau$	0.66 **	0.88 ***	0.01	0	0.68 **	0.91 **	0.01	0
	$\alpha + \sigma$	0.19	0.15	0.18 **	0.14*	0	0	0	0 **
	$\sigma$	0.7 **	0.43 **	0.55 ***	0.51 ***	0.22	0	0.2 ***	0 **
	$\alpha$	2.16 ***	1.95 ***	0.35 **	0.5 ***	1.88 ***	2.38 ***	0	0
	$\emptyset$	0.82 **	0.92 ***	0.01	0	0.85 **	0.88 **	0.01	0

e Log-variance of the latent field smoothing MSE.

		Type of data							
		$\alpha + \sigma + \tau$	$\sigma + \tau$	$\alpha + \tau$	$\tau$	$\alpha + \sigma$	$\sigma$	$\alpha$	$\emptyset$
Type of model	$\alpha + \sigma + \tau$	0	0	0	0	0	0	0 **	0 ***
	$\sigma + \tau$	0	0	0	0	0	0	0 ***	0 ***
	$\alpha + \tau$	0	0	0	0	0	0	0 **	0 ***
	$\tau$	0.09	0.02	0.01	0	0.08 ***	0.03 ***	0.01 ***	0 ***
	$\alpha + \sigma$	0.85 ***	0.79 ***	0.8 ***	0.83 ***	0	0	0	0
	$\sigma$	0.82 ***	0.81 ***	0.73 ***	0.84 ***	0	0	0	0
	$\alpha$	0.85 ***	0.74 ***	0.84 ***	0.83 ***	0	0	0	0
	$\emptyset$	0.84 ***	0.88 ***	0.85 ***	0.88 ***	0	0	0 **	0

f Log-variance of the noise smoothing MSE.

Table S4: Performance of the models with nonstationary range, noise, and field variance, in isotropic settings

Legend: “right model” ■; “wrong model” ■; “over-modeling” ■; “under-modeling” ■

\*\*\* :  $p < 2e - 16$ ; \*\* :  $p < 0.001$ ; \* :  $p < 0.01$

$\alpha$ : (locally isotropic) nonstationary range.  $\sigma$ : nonstationary latent field variance.  $\tau$ : nonstationary noise variance.  $\emptyset$ : full stationarity.

*Read: table S4a shows the results for latent field smoothing. The second column summarizes the experiments made with data sets presenting nonstationary variance in the latent field and noise, as indicates its column name “ $\sigma + \tau$ ”. The reference, in green, is the “right model” with the same specification. The associated coefficient is therefore 0. Just below, we can see the coefficient associated with the model  $\alpha + \tau$ . Its brown color tells that it is a “wrong” model. It adds, in average, 0.09 to the smoothing MSE with respect to the “right” model. The three p-value stars indicate  $p < 2e - 16$ .*

		Type of data							
		$\alpha + \sigma + \tau$	$\sigma + \tau$	$\alpha + \tau$	$\tau$	$\alpha + \sigma$	$\sigma$	$\alpha$	$\emptyset$
Type of model	$\alpha + \sigma + \tau$	1	1	1	0.92	1	0.95	0.95	0.89
	$\sigma + \tau$	0.46	1	0.36	0.97	0.45	0.97	0.29	0.81
	$\alpha + \tau$	0.16	0.07	1	0.93	0.02	0	1	0.86
	$\tau$	0.52	0.46	0	0.64	0.61	0.79	0.19	0.91
	$\alpha + \sigma$	0.98	0.98	1	1	0.98	1	1	0.88
	$\sigma$	0.52	0.88	0.43	0.85	0.53	0.93	0.33	0.88
	$\alpha$	0.25	0.02	0.83	0.71	0.03	0	1	0.91
	$\emptyset$	0.36	1	0.22	0.85	0.12	0.98	0.2	0.83

a Range intercept

		Type of data							
		$\alpha + \sigma + \tau$	$\sigma + \tau$	$\alpha + \tau$	$\tau$	$\alpha + \sigma$	$\sigma$	$\alpha$	$\emptyset$
Type of model	$\alpha + \sigma + \tau$	0.93	0.91	1	1	0.88	1	1	1
	$\sigma + \tau$	0.8	0.9	0.98	1	0.78	0.97	1	1
	$\alpha + \tau$	0	0	1	1	0.02	0	1	0.98
	$\tau$	0.15	0.03	0.3	1	0.17	0	0.41	0.98
	$\alpha + \sigma$	0.75	0.85	1	1	0.88	0.92	1	1
	$\sigma$	0.8	0.89	1	1	0.9	0.97	1	1
	$\alpha$	0	0	0.02	0	0	0	1	1
	$\emptyset$	0.02	0	0.5	1	0.02	0	0.69	1

b Field variance intercept

		Type of data							
		$\alpha + \sigma + \tau$	$\sigma + \tau$	$\alpha + \tau$	$\tau$	$\alpha + \sigma$	$\sigma$	$\alpha$	$\emptyset$
Type of model	$\alpha + \sigma + \tau$	0.97	0.95	0.9	1	1	1	1	1
	$\sigma + \tau$	0.86	0.93	0.8	0.98	1	1	1	1
	$\alpha + \tau$	0.97	1	0.82	0.98	1	1	1	1
	$\tau$	0.87	0.88	0.85	0.78	1	1	1	1
	$\alpha + \sigma$	0	0	0	0.02	0.98	1	1	1
	$\sigma$	0	0.02	0	0	1	1	0.93	1
	$\alpha$	0	0	0	0	0.83	0.86	1	1
	$\emptyset$	0	0	0	0	0.85	1	0.85	1

c Noise variance intercept

		Type of data							
		$\alpha + \sigma + \tau$	$\sigma + \tau$	$\alpha + \tau$	$\tau$	$\alpha + \sigma$	$\sigma$	$\alpha$	$\emptyset$
Type of model	$\alpha + \sigma + \tau$	1	0	1	0	1	0	1	0
	$\sigma + \tau$	0	1	0	1	0	1	0	1
	$\alpha + \tau$	0	0	1	0	0.02	0	1	0
	$\tau$	0	1	0	1	0	1	0	1
	$\alpha + \sigma$	0.46	0	0.26	0	1	0	1	0
	$\sigma$	0	1	0	1	0	1	0	1
	$\alpha$	0	0	0.25	0	0	0	1	0
	$\emptyset$	0	1	0	1	0	1	0	1

d Variance of the range's PP

		Type of data							
		$\alpha + \sigma + \tau$	$\sigma + \tau$	$\alpha + \tau$	$\tau$	$\alpha + \sigma$	$\sigma$	$\alpha$	$\emptyset$
Type of model	$\alpha + \sigma + \tau$	0.98	0.88	0	0	0.88	0.93	0	0
	$\sigma + \tau$	0.34	0.98	0	0	0.32	0.95	0	0
	$\alpha + \tau$	0	0	1	1	0	0	1	1
	$\tau$	0	0	1	1	0	0	1	1
	$\alpha + \sigma$	0.68	0.92	0	0	0.91	0.95	0	0
	$\sigma$	0.2	0.4	0	0	0.52	0.88	0	0
	$\alpha$	0	0	1	1	0	0	1	1
	$\emptyset$	0	0	1	1	0	0	1	1

e Variance of the field variance's PP

		Type of data							
		$\alpha + \sigma + \tau$	$\sigma + \tau$	$\alpha + \tau$	$\tau$	$\alpha + \sigma$	$\sigma$	$\alpha$	$\emptyset$
Type of model	$\alpha + \sigma + \tau$	1	1	0.98	0.98	0	0	0	0
	$\sigma + \tau$	1	1	1	1	0	0	0	0
	$\alpha + \tau$	1	0.98	1	1	0	0	0	0
	$\tau$	1	1	1	1	0	0	0	0
	$\alpha + \sigma$	0	0	0	0	1	1	1	1
	$\sigma$	0	0	0	0	1	1	1	1
	$\alpha$	0	0	0	0	1	1	1	1
	$\emptyset$	0	0	0	0	1	1	1	1

f Variance of the noise variance's PP

Table S5: Coverage of the parameters by 95% credibility intervals in the locally isotropic experiment.

Legend: “right model” ■; “wrong model” ■; “over-modeling” ■; “under-modeling” ■

\*\*\* :  $p < 2e - 16$ ; \*\* :  $p < 0.001$ ; \* :  $p < 0.01$

$\alpha$ : (locally isotropic) nonstationary range.  $\sigma$ : nonstationary latent field variance.  $\tau$ : nonstationary noise variance.  $\emptyset$ : full stationarity.

*Read: table S5e shows the coverage of the log-variance of the PP controlling the latent field's variance. The sixth column is named “ $\sigma$ ”, which means that the data was generated with a latent field whose variance is nonstationary. We can see that the “right” model, in green, has a coverage of 88 %. Models who have a nonstationary field variance and other(s) type(s) of nonstationarity as well, in blue on the same column, have a satisfying coverage, but the “wrong” models (in brown) or the under-modeling stationary model (in gray) model have a 0% coverage.*

		Type of data		
Type of model	A	$\alpha$	$\emptyset$	
A	0	0	0**	
$\alpha$	0.01***	0	0	
$\emptyset$	0.03***	0.02***	0	

a smooth field MSE

		Type of data		
Type of model	A	$\alpha$	$\emptyset$	
A	0	0.02	0**	
$\alpha$	0.5***	0	0*	
$\emptyset$	0.85***	0.66***	0	

b pred field MSE

		Type of data		
Type of model	A	$\alpha$	$\emptyset$	
A	0	0***	0***	
$\alpha$	0.69***	0	0	
$\emptyset$	0.69***	0	0	

d log range aniso MSE

		Type of data		
Type of model	A	$\alpha$	$\emptyset$	
A	0	2	-16**	
$\alpha$	218***	0	-14**	
$\emptyset$	612***	354***	0	

e DIC

Table S6: Performance in anisotropic settings

Legend: “right model” ■; “over-modeling” ■; “under-modeling” ■

\*\*\* :  $p < 2e - 16$ ; \*\* :  $p < 0.001$ ; \* :  $p < 0.05$

A: nonstationary anisotropic.  $\alpha$ : nonstationary isotropic.  $\emptyset$ : stationary

Read: in table a, giving results for the smoothing MSE, the left-hand column corresponds to nonstationary anisotropic data. The “right” model is then the nonstationary anisotropic model, called “A”, and it is the reference of the column, explaining that the upper-left coefficient is 0 and its color is green. The bottom-left coefficient is 0.03, meaning that using a stationary model instead of the “right” model will add 0.03 to the smoothing MSE. Its color is gray, indicating under-modeling. The three stars indicate that  $p < 0.001$ .

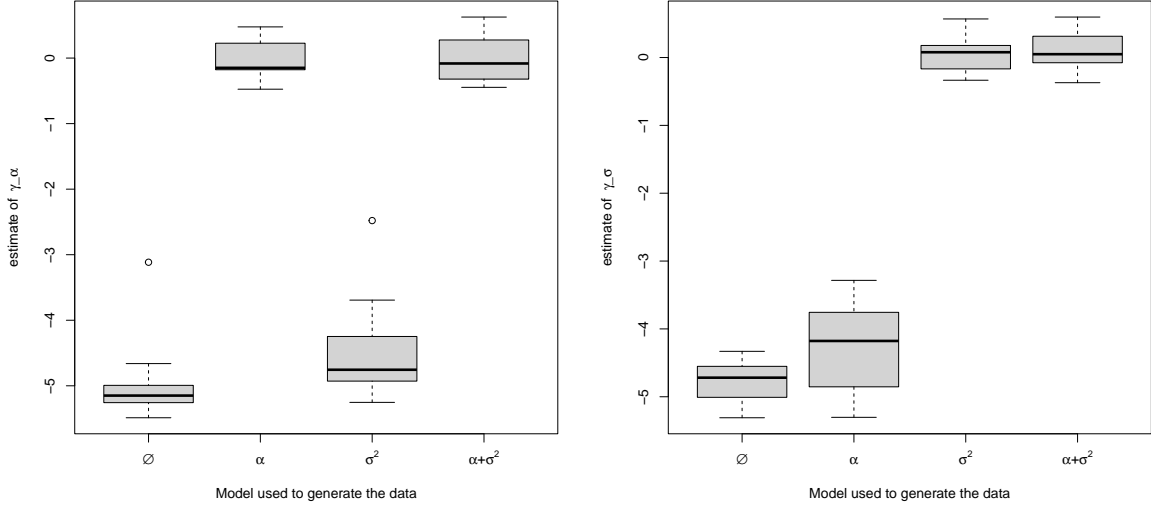
		Type of data					Type of data					Type of data		
		A	$\alpha$	$\emptyset$			A	$\alpha$	$\emptyset$			A	$\alpha$	$\emptyset$
Model	A	1	0.91	0.91	Model	A	0.92	0.96	0.98	Model	A	0.92	0.96	0.98
	$\alpha$	0.68	0.93	0.93		$\alpha$	1	1	1		$\alpha$	1	1	1
	$\emptyset$	0	0.2	0.88		$\emptyset$	1	1	1		$\emptyset$	1	1	1
	a range intercept 1					b range intercept 2					c range intercept 3			
		Type of data					Type of data					Type of data		
		A	$\alpha$	$\emptyset$			A	$\alpha$	$\emptyset$			A	$\alpha$	$\emptyset$
Model	A	0.86	0.89	0	Model	A	0.92	1	1	Model	A	0.9	0.94	0.98
	$\alpha$	0.85	0.92	0		$\alpha$	1	1	1		$\alpha$	1	1	1
	$\emptyset$	0	0	1		$\emptyset$	1	1	1		$\emptyset$	1	1	1
	d range log-var 1					e range log-var 2					f range log-var 3			
		Type of data					Type of data					Type of data		
		A	$\alpha$	$\emptyset$			A	$\alpha$	$\emptyset$			A	$\alpha$	$\emptyset$
Model	A	0.71	0	0	Model	A	0.9	1	1	Model	A	0.67	0	0
	$\alpha$	0	1	1		$\alpha$	1	1	1		$\alpha$	0	1	1
	$\emptyset$	0	1	1		$\emptyset$	1	1	1		$\emptyset$	0	1	1
	g range log-var 4					h range log-var 5					i range log-var 6			
		Type of data					Type of data					Type of data		
		A	$\alpha$	$\emptyset$			A	$\alpha$	$\emptyset$			A	$\alpha$	$\emptyset$
Model	A	0.94	0.96	0.89	Model	A	0.98	0.96	0.89	Model	A	0.98	0.96	0.89
	$\alpha$	0.92	0.93	0.9		$\alpha$	0.95	0.93	0.93		$\alpha$	0.95	0.93	0.93
	$\emptyset$	0.65	0.67	0.95		$\emptyset$	0.6	0.7	0.9		$\emptyset$	0.6	0.7	0.9
	j scale intercept					k noise intercept								

Table S7: Coverage of the parameters by 95% credibility intervals in the anisotropic experiment.

Legend: “right model” ■; “over-modeling” ■; “under-modeling” ■

\*\*\* :  $p < 2e - 16$ ; \*\* :  $p < 0.001$ ; \* :  $p < 0.05$

Read: *In table b, we can see that the second component of the range Intercept was covered by the 95% credibility intervals in 92% of the cases, when the data and the model are both nonstationary anisotropic. The green color tells us that this combination of model and data is “the right” formulation.*



(a) Estimates of the log variance for  $W_\alpha$

(b) Estimates of the log variance for  $W_\sigma$

Figure S1: Estimates of the log-variance of  $W_\alpha$  and  $W_\sigma$  in the model  $(\alpha + \sigma^2)$  following the type of the data

are supposed to be high. The predictive process spatial basis of size  $k$  is given as:

$$P = \tilde{R}_\theta^{-1}M,$$

$\tilde{R}_\theta^{-1}$  being a NNGP factor and  $M$  being a matrix of size  $n \times k$  such that  $M_{i,j} = 1$  if  $i = j$  and  $M_{i,j} = 0$  everywhere else. The  $k$  first spatial locations are called *knots* and they must be well-spread over the spatial domain in order to guarantee a good PP approximation. In our implementation, a K-means algorithm sets the knots automatically. Using fast solving relying on the sparsity and triangularity of  $\tilde{R}$ , computing  $P\beta = \tilde{R}_\theta^{-1}(M\beta)$  is affordable and avoids large matrix multiplications when  $\beta$  is a matrix with  $k$  rows and few columns.

We provide a few remarks on the selection of knots. The knots can be found as the centers of a K-means clustering, thereby allowing the user to specify only the desired number of knots. Our package vignette offers a quick look at how the PP samples behave using our spatial plotting functions. We point out that [Guhaniyogi et al. \(2011\)](#) have undertaken a rather thorough investigation of adaptive knot selection in predictive process models. For

now, our recommendation is to make the PP as simple as possible, and to keep in mind that even though we have not solved all our problems, we are able to work with a very large number of high-level parameters, which is an achievement in itself. In view of what we can achieve, the PP should more be seen as a very smooth P-spline rather than a fine approximation of a GP.

## S7 Lead data analysis

The lead data set presented by ? features various heavy metals measurements, including lead concentration. Various anthropic (density of air pollution, mining operations, toxic release, night lights, roads) and environmental (density of earthquakes, indices of green biomass, elevation, wetness, visible sky, wind effect) predictors are provided. These variables may impact the emission of the lead, its diffusion, or both. The lead concentration and the predictors have been observed on 58,097 locations, with a total of 64,274 observations. Figure S2 reveals that the measures are irregular, with large empty areas. The observations were transformed to the logarithmic scale.

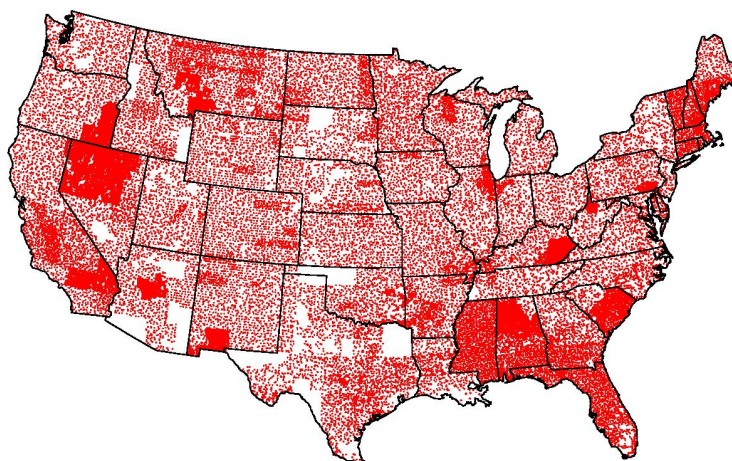


Figure S2: Measure sites for lead concentration

We used an NNGP with 10 neighbors and the max-min ordering (Guinness, 2018). We tested all the configurations ranging from a stationary model to a full nonstationary model, where noise, scale, and range may vary. The smoothness parameter was set to  $\nu = 1.5$ . The nonstationary parameters were modeled using environmental regressors and spatial effects. The spatial effects were specified using the Karhunen-Loève basis functions from a truncated expansion and solving for the eigenvalues and eigenvectors of the expansion from an approximate linear system over 500 knots. Curiously, the predictive process emerges from this solution (see, e.g., Chapter 12 in Banerjee et al., 2014). The range and the marginal variance were also explained using the most spatially coherent regressors (elevation, green biomass index, and wetness index), while the noise was modeled with all the regressors.

The models are compared using the DIC, the mean log-density of the observations, and the mean log-density of the predictions, the MSE of the latent field being unavailable for this real data set. We used 50,000 spatial locations for training the model, holding out the rest for prediction. The MCMC convergence was monitored using univariate Gelman-Rubin-Brooks diagnostics (Gelman et al., 1992; Brooks and Gelman, 1998) of the high-level parameters (all the parameters of the models except the latent field  $w(\mathcal{S})$ ). Unsurprisingly, more complex runs required larger number of iterations to converge.

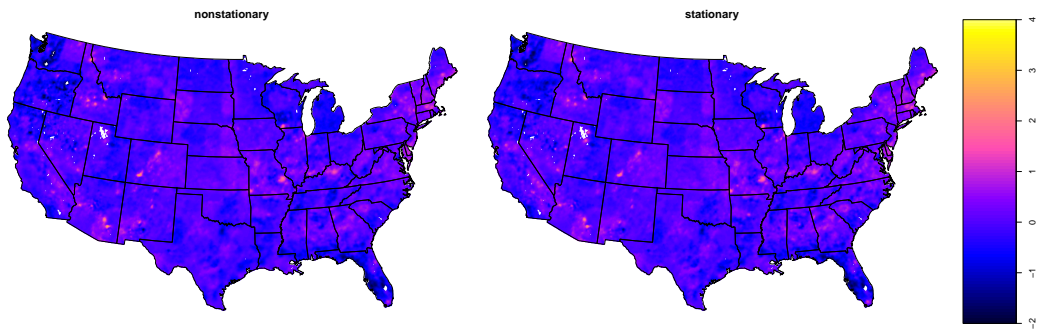
Table S8 summarizes a few model assessment metrics for the lead data analysis. The point that clearly differs from the synthetic experiments presented in the main manuscript is that the most complex model does not necessarily excel over simpler models, although it performs better than the stationary model according to all the criteria. Indeed, the model  $\alpha + \sigma + \tau$  is bested by  $\alpha + \tau$ ,  $\sigma + \tau$ , and  $\tau$  in predicting at unobserved locations. We, however, note that the best model falls within one of the formulations recommended at the end of section 5.1: A model with either nonstationary range or variance for the latent field and nonstationary noise. It is also confirmed that a poorly formulated nonstationary model leads to significant overfitting: omitting the noise variance  $\tau$  results in a clear improvement of the DIC and

Table S8: Comparison of the runs for the lead analysis

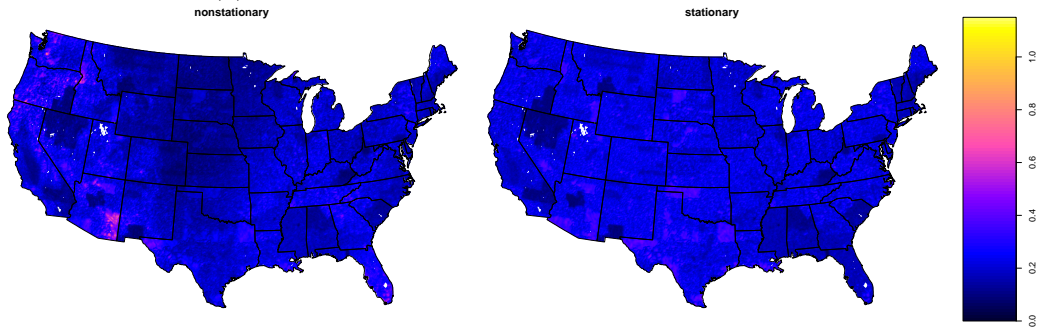
Model	prediction	smoothing	DIC	time (minutes)	number of iterations
$\alpha + \sigma + \tau$	-0.775	-0.515	65706	190	3000
$\alpha + \tau$	-0.736	-0.535	66797	185	3000
$\sigma + \tau$	-0.716	-0.551	67964	87	2000
$\tau$	-0.725	-0.562	68808	85	2000
$\alpha + \sigma$	-1.294	-0.415	62660	120	2000
$\alpha$	-1.166	-0.448	64887	120	2000
$\sigma$	-0.910	-0.555	72243	91	2000
$\emptyset$	-0.787	-0.642	78157	45	1000

the log-density at observed locations, but is compromised by a sharp degradation of the log-density at unobserved locations.

The predicted mean and standard deviation of the latent field are presented in Figure S3 with a comparison between the stationary and the best nonstationary model. The mean nonstationary parameters are presented in Figure S4 with a decomposition between the part explained by environmental covariates and the part explained by spatial effects. While the predicted means are quite similar between the stationary and nonstationary models (Figure S3(a)), the predicted standard deviations are substantially different (Figure S3(b)). The standard deviation of the stationary model's predictions depends upon the density of the observations. The denser the observations in one region, the smaller the standard deviation. Meanwhile, the standard deviation of the nonstationary model's predictions takes the local properties of the process into account. Note, for example, that the United States mid-west has a lower standard deviation in spite of spatial sampling being rather sparse. Also, we point out two gaps in the spatial sampling domain, one in South-East Arizona and another in North-West Oklahoma, where they have a very different predicted standard deviation albeit having the same size.

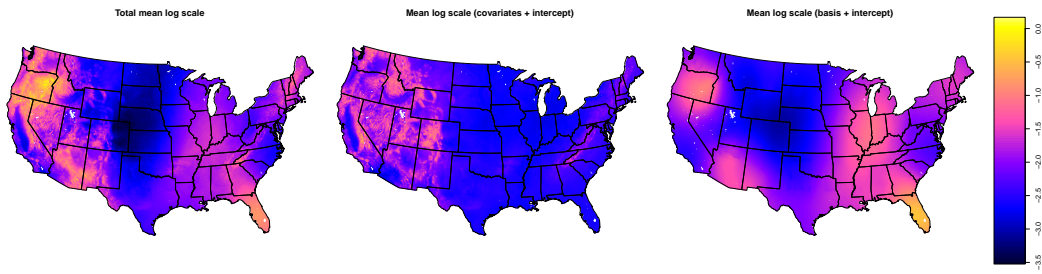


(a) Predicted latent mean of the lead concentration

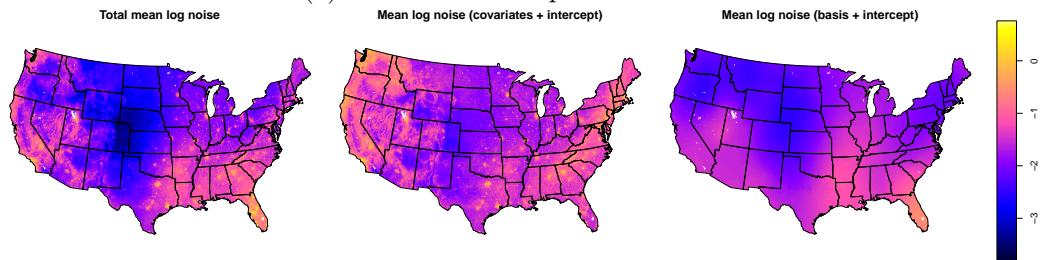


(b) Predicted latent standard deviation of the lead concentration

Figure S3: Predicted mean and standard deviations of the latent field for the stationary and nonstationary models.



(a) Predicted latent process variance



(b) Predicted noise variance

Figure S4: Predicted mean of the covariance parameters in the selected nonstationary model.